The Dissertation Committee for Ann M. Clemens Certifies that this is the approved version of the following dissertation:

ADAPTIVE RESPONSES TO CELLULAR STRESS IN NEURONS OF THE HIPPOCAMPUS

Committee:

Daniel Johnston, Supervisor

Kristen M. Harris, Co-Supervisor

Richard W. Aldrich

Chandrajit L. Bajaj

Hiroshi Nishiyama

ADAPTIVE RESPONSES TO CELLULAR STRESS IN NEURONS OF THE HIPPOCAMPUS

by

Ann M. Clemens, B.S. Bio.

Dissertation

Presented to the Faculty of the Graduate School of

The University of Texas at Austin

in Partial Fulfillment

of the Requirements

for the Degree of

Doctor of Philosophy

The University of Texas at Austin

August 2013

Dedication

To my parents.

Acknowledgements

First and foremost, I thank my advisor, Dr. Daniel Johnston for his generous support, patience and guidance. He gave me the freedom to explore a wide range of ideas and scientific paths, some succeeded and some failed, but he continued to express his confidence and faith in me. I consider the things that I learned along the way to be far more valuable than if I had been pointed to the shortest, most direct route to the PhD. I am exceedingly grateful for the tremendous resources and kind encouragement that he has given me over the years.

I would also like to thank my co-advisor Dr. Kristen Harris for supporting me in the initial phase of my graduate work. In her lab, I learned a great deal about transmission electron microscopy and dendritic ultrastructure. She has always been very warm and understanding, even when my initial goal to carry out a project in retrospective serial section electron microscopy did not pan out.

Special thanks also go to Dr. Rick Aldrich for serving as a committee member, teacher and for allowing me to rotate in his lab. My chats with Rick have never failed to be inspirational, whether it be in regards to science, music, life or other. I would also like to extend my thanks to Dr. Hiroshi Nishiyama and Dr. Chandra Bajaj for serving on my thesis committee, for their continued interest in this research project and personal encouragement at all steps along the way.

I am extremely grateful to the members of the Johnston laboratory, both past and present, for always offering valuable feedback and providing for a stimulating and enjoyable scientific environment. Thanks to Dr. Rishi Narayanan for his input and discussions while in Austin and continued email correspondence from India. Thank you to Dr. Randy Chitwood who helped me with my initial retrospective EM efforts and has continued to provide me with much appreciated feedback and support. Thanks to Dr. Kelly Dougherty and Dr. Ruchi Malik for always being available to discuss things dorso-ventral, for offering advice on writing and presentations, and for being good friends. I would especially like to thank Dr. Sachin Vaidya and Dr. Rick Gray for their unprecedented support and friendship along the way. From them, I learned the value of having lab mates that will never hesitate to tell you when you're wrong, always offer help when you need it and never fail to make you laugh when you're down. Additional thanks to Drs. Brian Kalmbach, Yul Young Park, Nikolai Dembrow, Gayathri Ranganathan, Chung Sub Kim, Darrin Brager, Jenni Siegel and Niraj Desai; as well as, Eedann McCord, Vicky Moya, Liz Arnold, Kathleen Pantalion and Krystal Phu; all of whom have contributed to my graduate work and life in some way.

Finally, I thank my brothers Mike and Alex and my parents Edna and Jim for their unconditional love and support. Without them, this would not have been possible.

ADAPTIVE RESPONSES TO CELLULAR STRESS IN NEURONS OF THE HIPPOCAMPUS

Ann M. Clemens, Ph.D.

The University of Texas at Austin, 2013

Supervisor: Daniel Johnston

Co-Supervisor: Kristen M. Harris

Disruptions of endoplasmic reticulum (ER) Ca^{2+} homeostasis are heavily linked to neuronal pathology. Depletion of ER Ca^{2+} stores can result in cellular dysfunction and potentially cell death, although adaptive processes exist to aid in survival. This dissertation examines the age and region-dependence of one postulated adaptive response to ER store depletion, store depletion (SD) HCN channel plasticity, in neurons of the dorsal (DHC) and ventral (VHC) hippocampus from adolescent and adult rats. Using whole-cell patch clamp recordings from the soma and dendrites of CA1 pyramidal neurons, the change in *h*-sensitive measurements in response to store depletion, induced by treatment with cyclopiazonic acid (CPA), a sarco/endoplasmic reticulum Ca^{2+}-ATPase blocker were observed. While DHC and VHC neurons in adolescent animals responded to store depletion with a peri-somatic expression of SD *h* plasticity, it was found that adult animals express SD *h* plasticity with a dendritic and somato-dendritic

locus of plasticity in DHC and VHC neurons, respectively. Furthermore, SD *h* plasticity in adults was dependent on membrane voltage and on the activation of *L*-type voltage gated Ca^{2+} channels. These results suggest that cellular responses to the impairment of ER function, or ER stress, are dependent upon brain region and age, and that the differential expression of SD *h* plasticity could provide a neural basis for region and age-dependent disease vulnerabilities.

Table of Contents

List of Tables

List of Figures

Chapter 1: Introduction

I. The balance between cellular stress and adaptation

The ability to adapt to stress is one of the most basic needs for living organisms. In support of this notion is the existence of highly conserved, complex adaptive pathways in nearly every cell type. The heat shock response, for example, which is common to bacteria and eukaryotes, is a response to unfolded proteins caused by elevated temperatures, oxidative stress, and heavy metals. This response, initiates a pathway of chaperone molecules that inhibit apoptosis and promote survival through enhanced protein folding and the alleviation of aggregated proteins (Fulda et al., 2010). DNA damage, which can be caused by irradiation, and oxidation, initiates the DNA damage response, which involves the activation of a multitude of enzymes, aimed at DNA remodeling and repair (Ciccia and Elledge, 2010). The unfolded protein response (UPR) occurring in a variety of endomembrane containing organisms including yeast, fungi, plants, protozoa, metozoa and mammals, is an adaptation to misfolded proteins that can arise as a result of many cellular stressors including glucose deprivation, disturbance of Ca^{2+} homeostasis and hypoxia (Hollien, 2013). A balance between adaptation and cellular stress must be maintained in order to prevent pathology (Fig.1). Exposure to stress inducing elements such as hypoxia, unfolded proteins, over-

excitation and intracellular Ca^{2+} depletion must be countered by adaptive processes. Factors that influence the capacity of adaption such as age, location in a certain brain region, injury and genetics are, thus, key to understanding why cellular stress is sometimes neutral and other times destructive.

II. Failures in adaptation propagate disease.

Failures of adaptation in small groups or even single neurons are capable of having catastrophic effects on brain function. Networks of the brain are highly interconnected, thus, dysfunction in one brain region should not be considered an isolated event. Acute injury to one group of neurons, for example, could have a dramatic impact on the output of a neighboring network when the injured region was heavily interconnected with this neighboring region (Fig. 2). Early compensatory engagement of other networks of neurons could make up for this loss, but if additional factors contribute to the impairment of these adaptive processes, the disruption of function could become widespread (Palop et al., 2006). This theoretical perspective on the origin and progression of disease is supported by the fact that such a vast number of neurodegenerative diseases are progressive. Alzheimer's disease, Parkinson's disease and Huntington's disease (to name a few) begin by affecting small groups of neurons, having subtle effects on cognition, but can go on to cause widespread neuronal damage with debilitating effects on behavior (Saxena and Caroni, 2011).

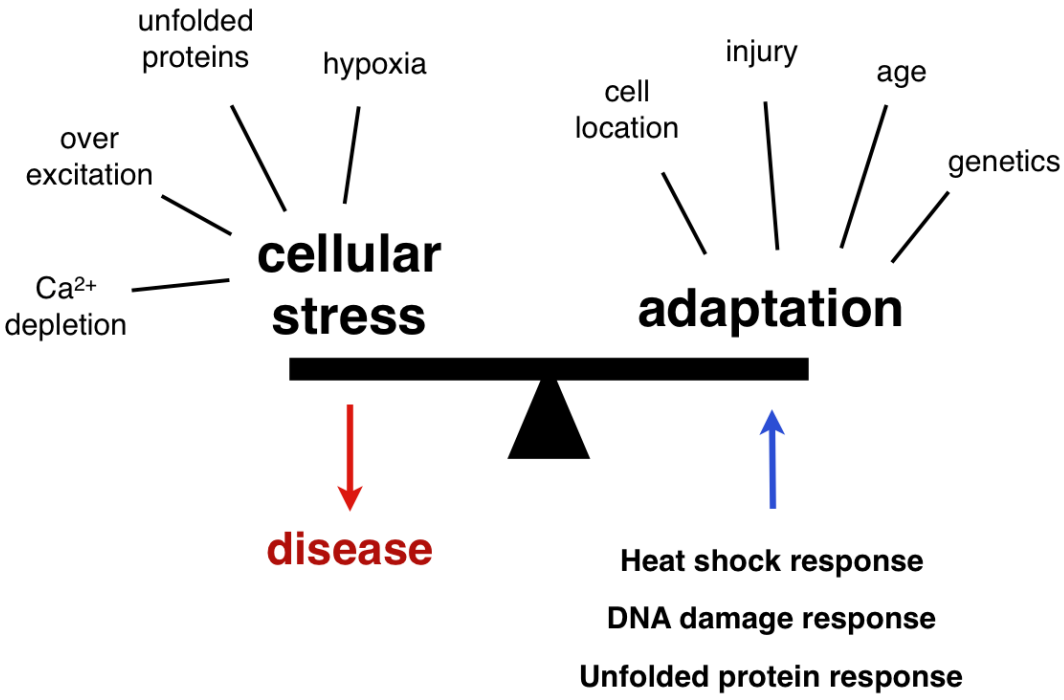

Figure 1: Balance between cellular stress and adaptation

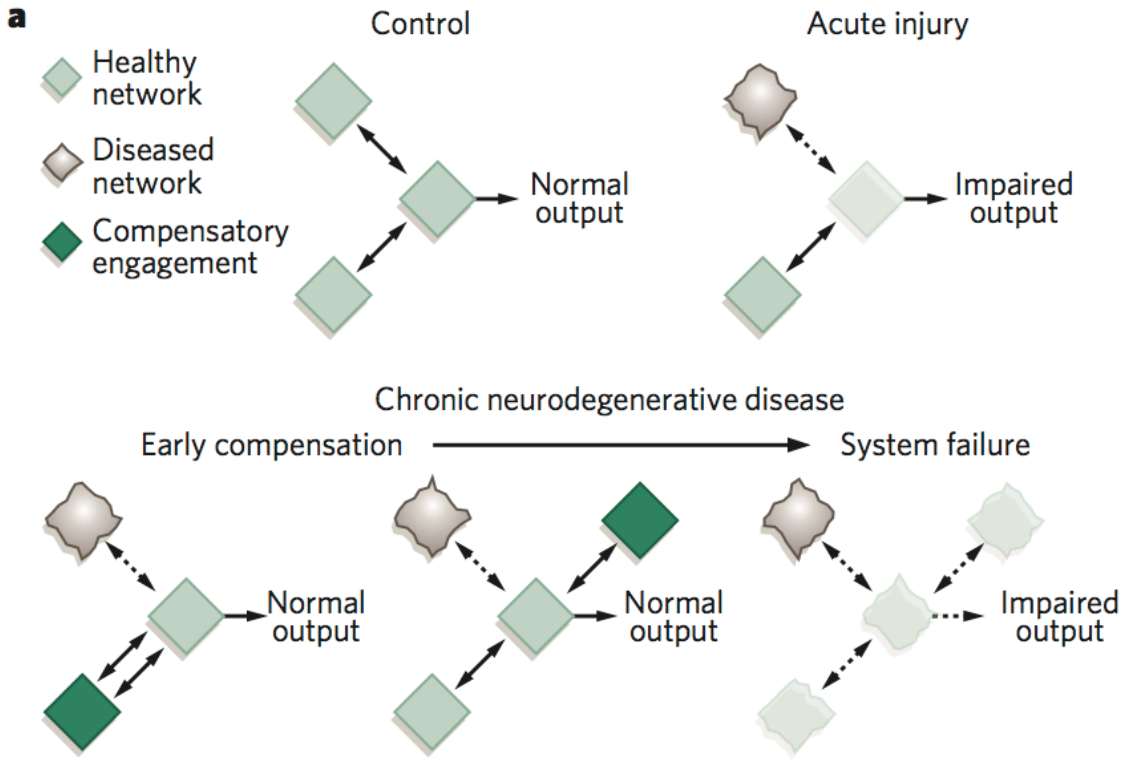

Figure 2: Interaction between neuronal adaptation and disease

Schematic for how neuronal adaptation could counteract disorders of the brain (Palop et al., 2006).

II. Endoplasmic reticulum stress and Ca^{2+} store depletion

One consequence that is common to neuronal stress and neurological disorders is the disruption of function of the endoplasmic reticulum (ER). Thus, the ER and ER-associated adaptive processes are central to our understanding of the relationship between stress, adaptation and disease in the brain.

A. Structure and function of the endoplasmic reticulum

The ER is a membrane-bound organelle found inside mammalian cells that contains a high concentration of Ca^{2+} (μM range) relative to the cytoplasm (nM range). This internal supply of Ca^{2+}, along with that contained within mitochondria, are known as the Ca^{2+} stores. It is proposed that early in evolution of eukaryotic cells, cells internalized a portion of the outer cellular membrane, forming the inner membrane system of the ER in order to facilitate the need for an internal compartment where protein processing, handling and transport could occur (Alberts, 2008). Subsequent to the assimilation of this endo-membrane system, the ER has become a ubiquitous component of mammalian cells that serves a multitude of functions including lipid synthesis and processing, the regulation of biochemical signaling processes, the assurance of proper protein handling and the maintenance of cellular Ca^{2+} homeostasis (Berridge, 2002).

In neurons, the ER forms a continuous network that extends from the nuclear membrane throughout the dendritic tree (Terasaki et al., 1994). The network of tubules and filaments that make up the ER is highly complex and specialized. In CA1 hippocampal neurons (Fig. 3), the ER extends into specific spine types (Spacek and Harris, 1997) and may assume complex structural arrangements to regulate trafficking of proteins within specialized dendritic compartments (Cui-Wang et al., 2012).

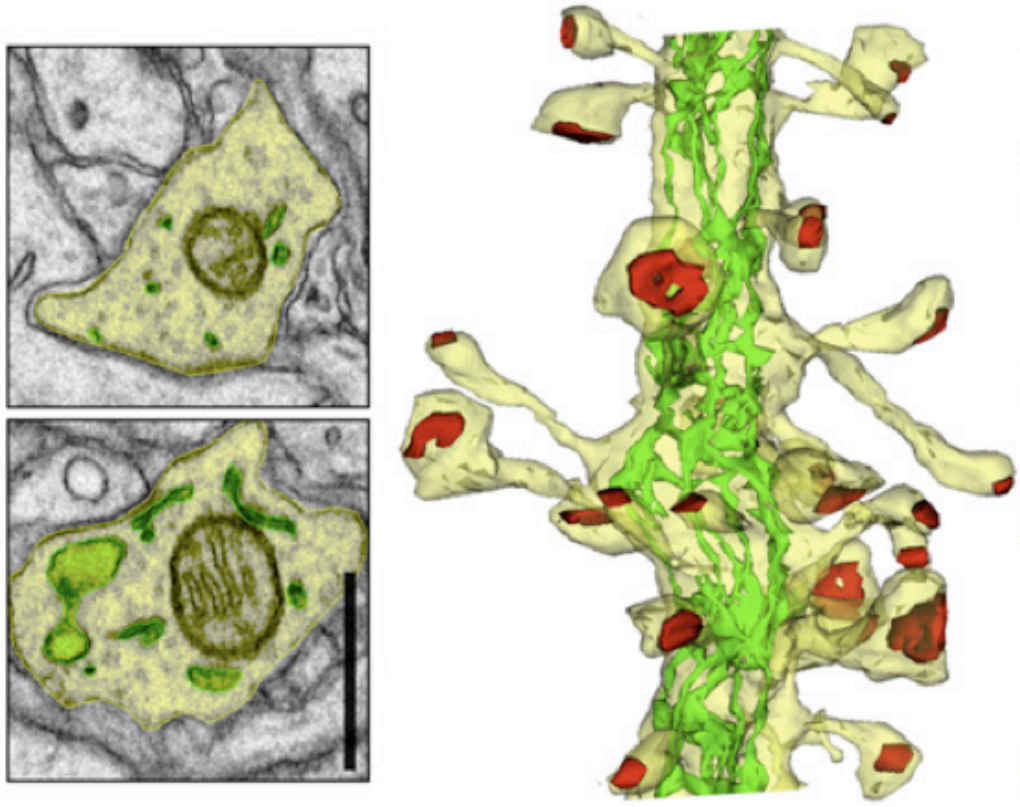

Figure 3: The endoplamic reticulum in neurons

The endoplamic reticulum in neurons forms a continuous structure that connects the nucleus with the dendritic processes. This example of dendritic ER, reconstructed in a CA1 pyramidal neuron of the hippocampus shows the complex network or tubules and filaments that make up this endomembrane system. Single sections of transmission electron microscopic (TEM) images of cross-sectioned apical dendrites (left) show how the ER (in green) can be highly variable in structure and location within the dendrite (scale bar represents 1 μm). 3D reconstruction of serial sectioned TEM images further exemplifies the complexity of the ER in a small dendritic segment (Cui-Wang et al., 2012).

B. Adaptations and responses to endoplasmic reticulum stress

The ER Ca^{2+} stores are highly linked to disorders of the brain. Disruptions of ER Ca^{2+} are associated with diseases that include (but are not limited to) ischemia, Alzheimer's disease, epilepsy, neuronal infection by the human immunodeficiency virus (HIV), diabetes, Parkinson's disease, Huntington's disease and physical neuronal trauma (Verkhratsky, 2005). Imbalances in protein handling that exceed the capacity of the ER result in the condition known as ER stress. Markers of ER stress may be initiated with a variety of stimuli including accumulation of unfolded proteins, depletion of ER Ca^{2+} stores, viral infection, over-excitation, hypoxia, sleep deprivation and physical neuronal trauma.

The unfolded protein response

The unfolded protein response (UPR) is a reaction to ER stress that aims to reduce the protein load on the ER by enhancing protein folding, inhibiting translation and promoting degradation of misfolded proteins. Although the goal of the UPR is initially to promote adaptation and cellular survival, if ER stress is prolonged the UPR will revert to apoptotic signaling and potentially cell death (Xu, 2005; Ron and Walter, 2007). Stress to the ER may activate one of the ER stress receptors including the PKR-like ER kinase (PERK), activating transcription factor 6 (ATF6) or the inositol-requiring enzyme 1 (Ire1) (Fig. 4)

(Fulda et al., 2010). These ER stress receptors effectively turn down protein translation, initiate chaperones to aid in protein folding and turn down the protein load in the ER to aid in the recovery from this accumulation of misfolded proteins.

When the protein load on the ER is too high or these adaptive pathways fail, the UPR reverts to apoptotic or necrotic signaling and cellular death ensues. The factors that might cause an adaptive process such as the UPR to fail are unclear, though substantial evidence shows that the UPR undergoes significant age-dependent modification.

Store operated Ca^{2+} entry

Store operated Ca^{2+} (SOC) entry is a Ca^{2+} refilling mechanism that is initiated by the depletion of Ca^{2+} from the ER. When stromal interaction molecule (STIM) proteins positioned within the ER lumen sense low levels of Ca^{2+}, they respond by forming a dimer and associating with two Orai tetramers located on the plasma membrane (Fig. 5). SOC entry, sometimes also referred to as capacitative Ca^{2+} entry has been recognized for decades, but a resurgence of interest has come with the molecular identification of its constituents (Luik et al., 2008; Cahalan, 2009). SOC entry, which was previously thought to be a method for non-excitable cells to mediate Ca^{2+} entry, has more recently been recognized as an important internal Ca^{2+} source in neurons. SOC entry and its constituents have not been extensively examined in states of disease, though SOC Ca^{2+} entry

is diminished in models of Alzheimer's disease and appears to be related to pathologies related to environmental toxins (Parekh, 2005).

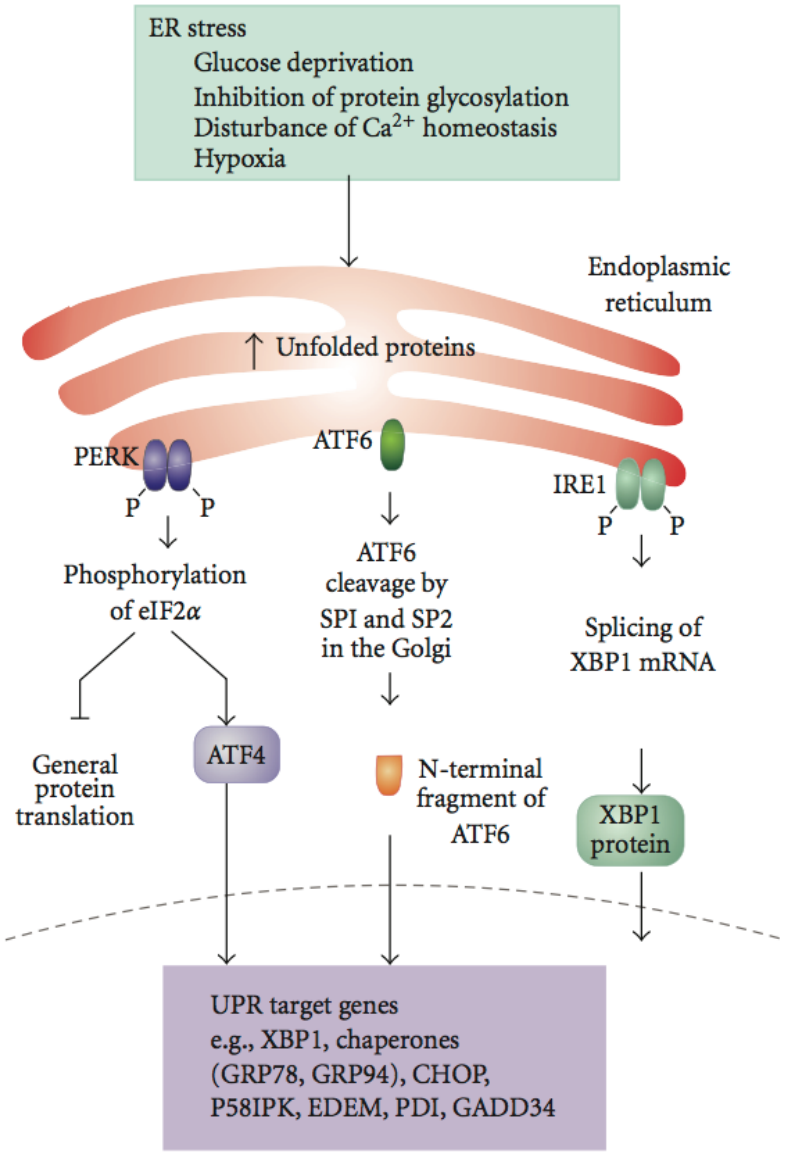

Figure 4: The unfolded protein response

The unfolded protein response (UPR) is initiated in response to a variety of cellular stressors, which ultimately result in an accumulation of unfolded proteins in the ER. This stress on the ER may initiate one of the ER stress receptors including the PERK, ATF6 or IRE1 receptors. These ER stress receptors effectively turn down protein translation, initiate chaperones to aid in protein folding and turn down the protein load in the ER (Fulda et al., 2010).

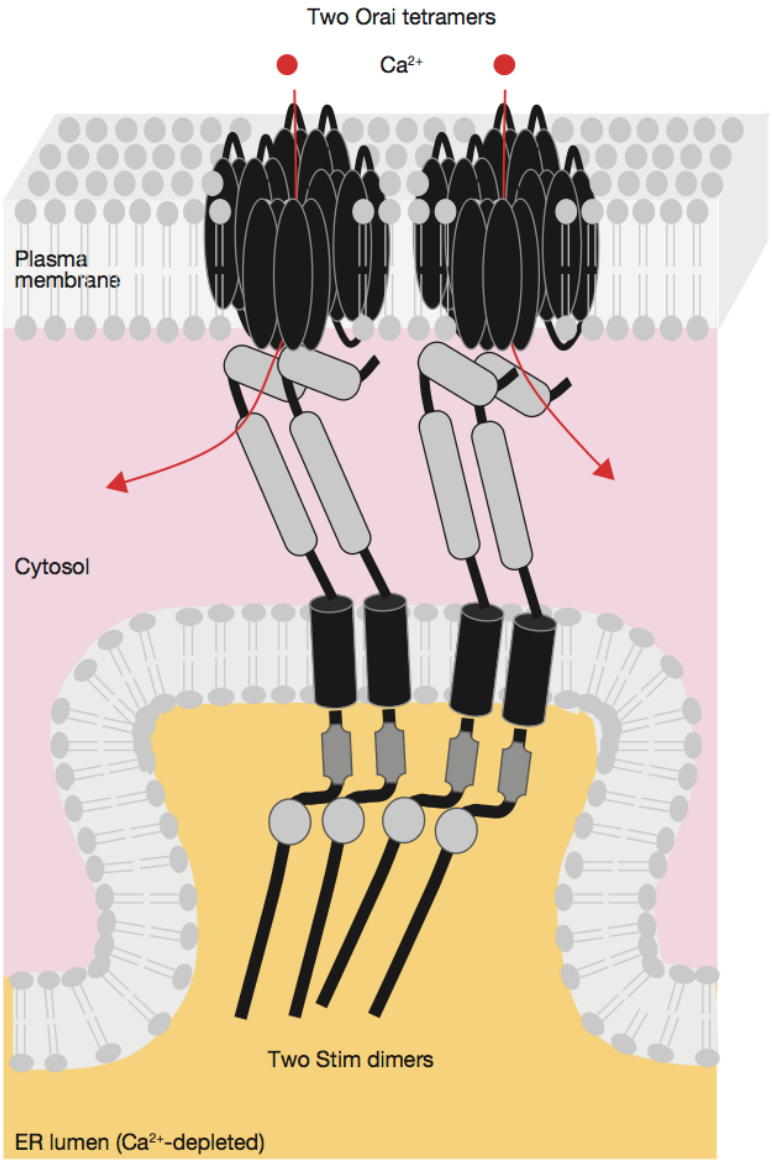

Figure 5: Store operated Ca^{2+} entry

The machinery involved in store operated Ca^{2+} (SOC) entry involves the association of two stromal interaction molecule (STIM) dimers located on the ER membrane with two Orai dimers located on the plasma membrane. Once this association is formed, Ca^{2+} from the extracellular space is recruited to the cytosol and subsequently sequestered to the ER (Cahalan, 2009).

IV. Store depletion *h* plasticity

A. The *h* current

Hyperpolarization and cyclic nucleotide gated (HCN) channels, or *h* channels, mediate the *h* current (I_h). I_h consists of a mixed inward cationic current carried by Na^+ and K^+, making its reversal potential around –20 mV under physiological conditions. As its name implies, the *h* current is activated with hyperpolarizing voltage steps (Fig. 6) and is modulated by cyclic nucleotides such as cyclic AMP.

Structurally, HCN subunits consist of six transmembrane domains where segment 4 (S4) is the voltage sensor and the C-terminus forms a cyclic nucleotide-binding site (Fig. 7). The channel forms a tetramer in cellular membranes (Biel et al., 2009). In hippocampal neurons, HCN1 and HCN2 are predominant subtypes. The *h* current, measured using cell-attached patch recordings, shows an increased density with distance from the soma in CA1 pyramidal neurons (Fig. 8) (Magee, 1998).

The physiological impact of *h* channels is to limit excitability and regulate the frequency response properties of cellular membranes (Fig. 9). The way that these physiological effects arise is due to the unique biophysical properties of the *h* channel. Due to the fact that I_h is active around the resting potential for most neurons, it is able to set the resting potential. In the case of some neuron types

that exhibit intrinsic oscillations or pace making, there may be an interaction of I_h and a depolarization-activated conductance. Interestingly, I_h can exhibit a depolarizing influence by activating with hyperpolarization from rest and have an effective hyperpolarizing effect by deactivating when the membrane potential depolarizes from rest. This is well illustrated by the example membrane deflections in Fig. 9A. With an increase in I_h, there is a reduction in the voltage deflection for current injections in the hyperpolarizing and depolarizing direction, which effectively reduces the cellular input resistance (R_{in}). A direct result of this reduction in input resistance is a reduction of neuronal firing (Fig. 9B).

I_h also has an influence on neuronal resonance, which is the preferential response of a neuron to a particular frequency. The resonance frequency of neurons can be determined by injecting an oscillating current injection of increasing frequency and then taking the Fourier transform of the voltage response to determine the frequency at which the impedance amplitude is largest (Fig. 9C). The band-pass filtering effect observed (Fig. 9 C,right) is due to a combination of the low-pass filtering of the membrane time constant (τ_m) and the high-pass filtering effect of I_h. I_h opposes changes in membrane voltage in the low frequency range, but as the frequency of the *Chirp* stimulus increases, the kinetics of *h* cannot keep up. If there is an overall increase in I_h, the high-pass filtering effects are augmented, resulting in an increase in resonance frequency (f_R).

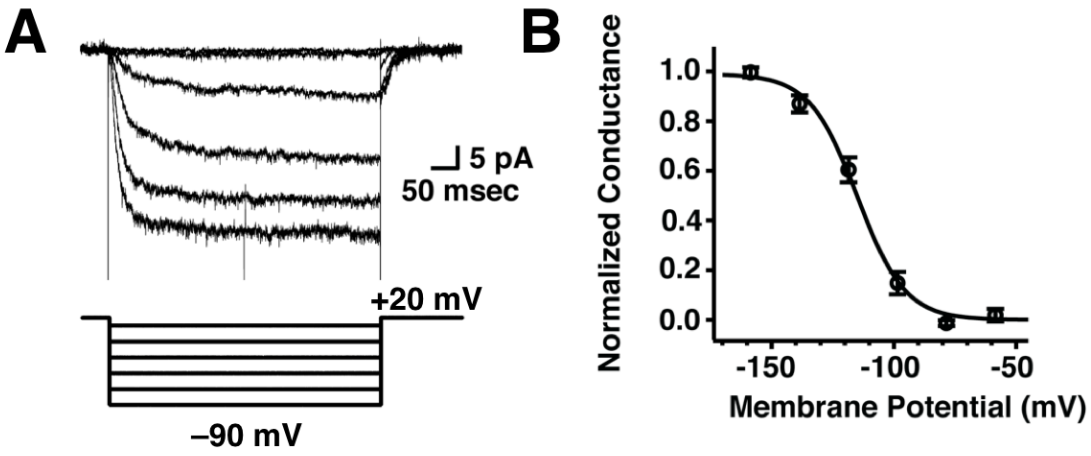

Figure 6: The *h* current activates with hyperpolarization.

(A) Hyperpolarizing voltage steps (relative to resting membrane potential) from a holding potential of +20 mV elicit an increasing *h* current. (B) Conductance-density plot constructed from peak tail currents. Figure courtesy of Kelly Dougherty.

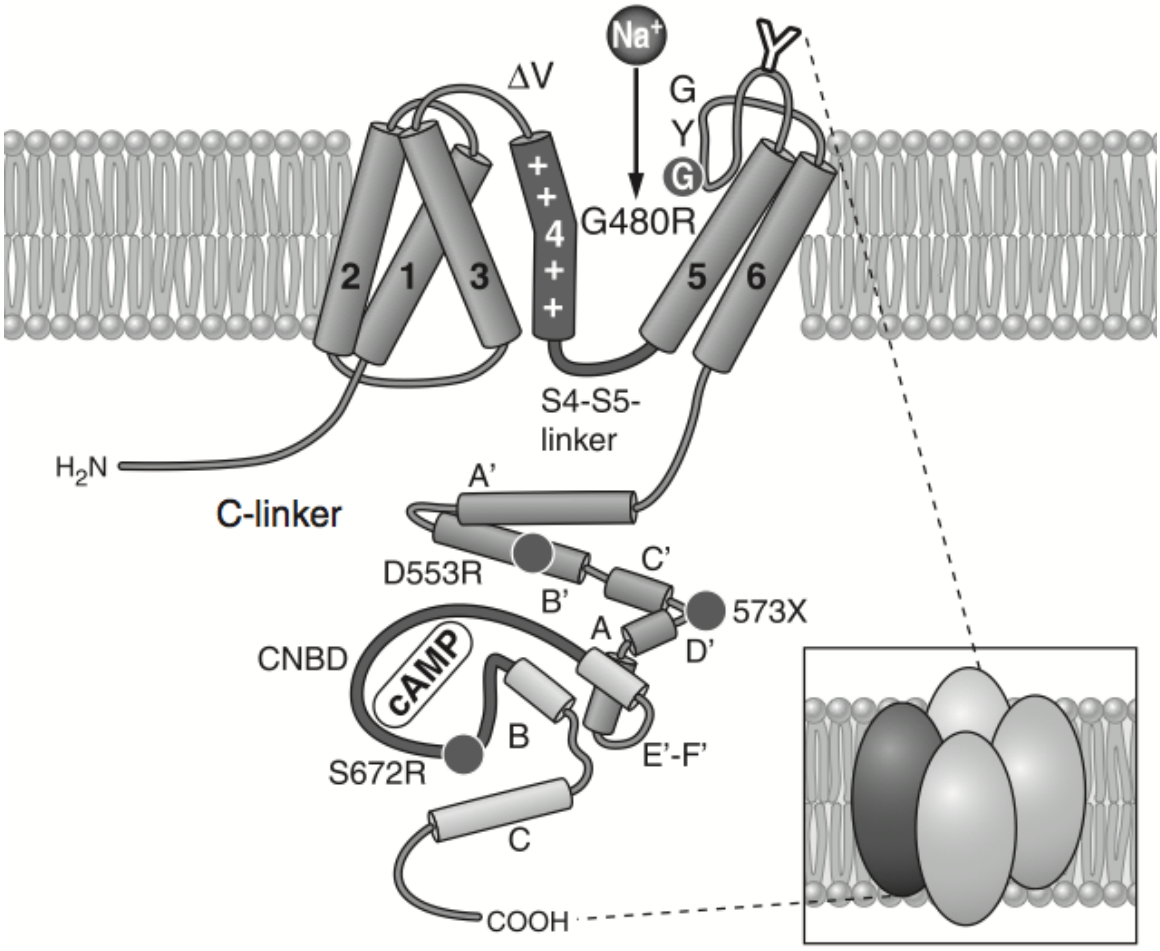

Figure 7: Structure of the *h* channel

Structure of the HCN subunit consists of 6 transmembrane domains where S6 is the voltage sensor and the cyclic nucleotide-binding domain is near the C-terminus. Each h channel is formed by a tetramer of HCN subunits (Biel et al., 2009).

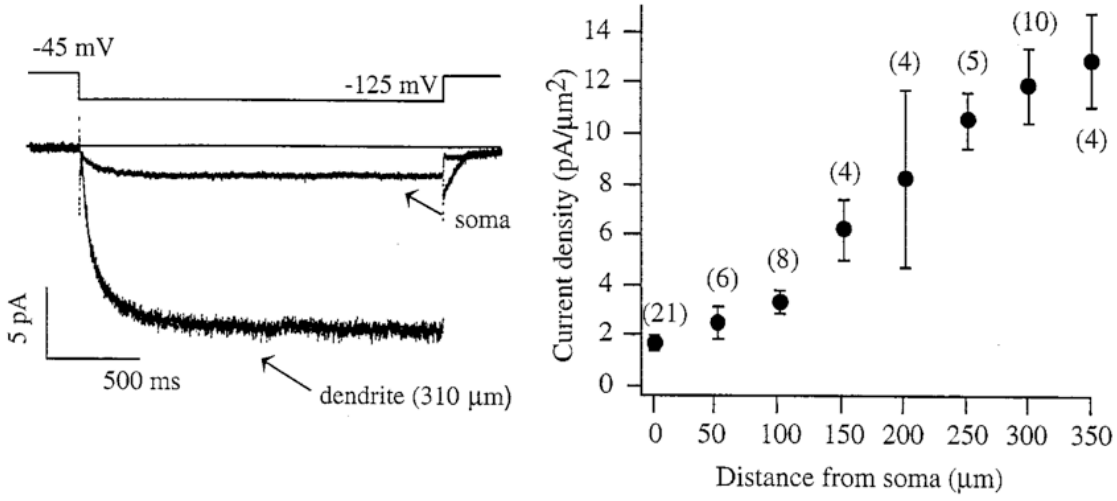

Figure 8: Density of the *h* current in the soma and dendrites of CA1 hippocampal neurons

Cell-attached patch voltage-clamp recordings of I_h from the dendrites of CA1 pyramidal neurons (Magee, 1998).

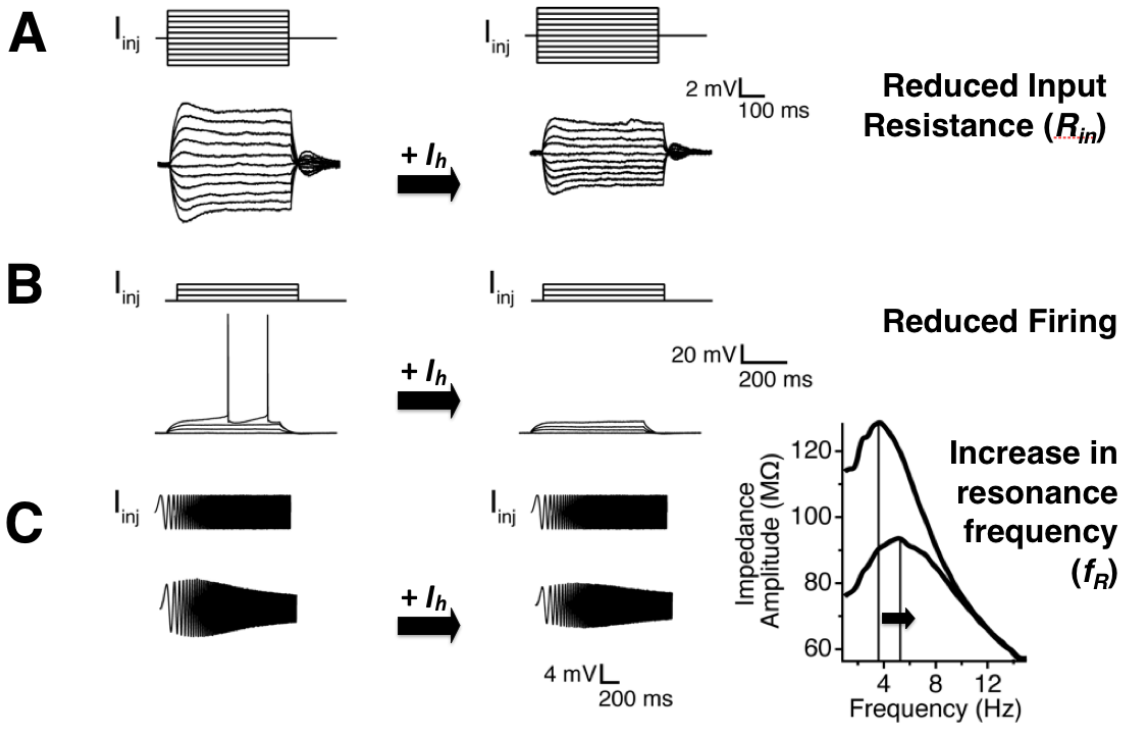

Figure 9: Effect of an increase in I_h on neuronal response properties

(A) Example traces showing a reduction in input resistance that would be expected due to an increase in I_h. Current steps range from –50 to +50 pA with 10 pA increments. (B) Example firing pattern before and after an increase in I_h. Current steps range from 0 pA to 150 pA in 50 pA increments. (C) Example voltage responses to a Chirp stimulus 100 pA in amplitude. The transform of these voltage responses to the frequency domain (right) showing the increase in resonance frequency expected from an increase in I_h.

B. Details of store depletion *h* plasticity

Recently, members of the Johnston laboratory showed that ER Ca^{2+} store depletion initiates a change in the intrinsic response properties of neurons that is mediated by a change in *h* channels. Specifically, depletion of the Ca^{2+} stores by application of the store depletion agents cyclopiazonic acid (CPA) for a short period of time (10 min.) caused a long-term reduction of intrinsic excitability, which was measured by a reduction in input resistance and a reduction in firing (Fig. 10B,C). Consistent with an increase in functional I_h, store depletion also caused an increase in the neuronal resonance frequency over time (Fig. 10D).

Store depletion (SD) *h* plasticity was mediated by an increase in the functional density, and a depolarizing shift in the activation range, of the *h* current (Fig. 11A—C). This change was not observed when measured 100 μm from the soma (Fig. 11D). Previous descriptions of *h* plasticity were described to be global (Narayanan and Johnston, 2007), though SD *h* plasticity appeared to only involve the peri-somatic region of the observed neurons. It was determined that SD *h* plasticity was dependent on Ca^{2+} release through inositol 1,4,5 trisphosphate receptors ($InsP_3Rs$), SOC entry and activation of protein kinase A (PKA) (Fig. 12). The peri-somatic location of plasticity was postulated to be due to the InsP3R-interacting molecule chromogranin B (CGB) (Schmidt and Ehrlich, 2010), which increases the open probability of the InsP3R and is expressed in the soma and proximal dendrites of hippocampal neurons (Jacob et al., 2005).

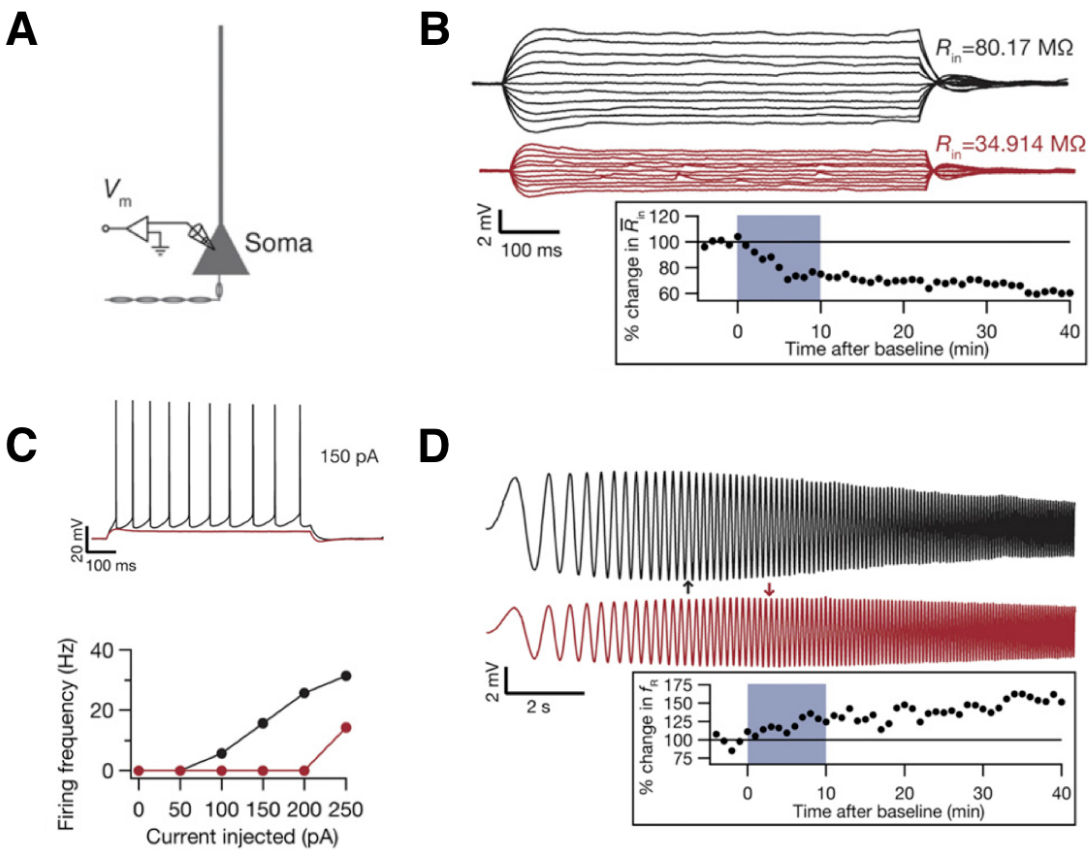

Figure 10: The effect of store depletion on the intrinsic response properties of CA1 neurons

(A) Whole-cell somatic patch clamp recordings were made from CA1 pyramidal neurons of the hippocampus. Store depletion induced by a 10 min. application of cyclopiazonic acid (CPA) caused a significant decrease in input resistance (B), reduction in firing (C) and increase in resonance frequency (D) (Narayanan et al., 2010a).

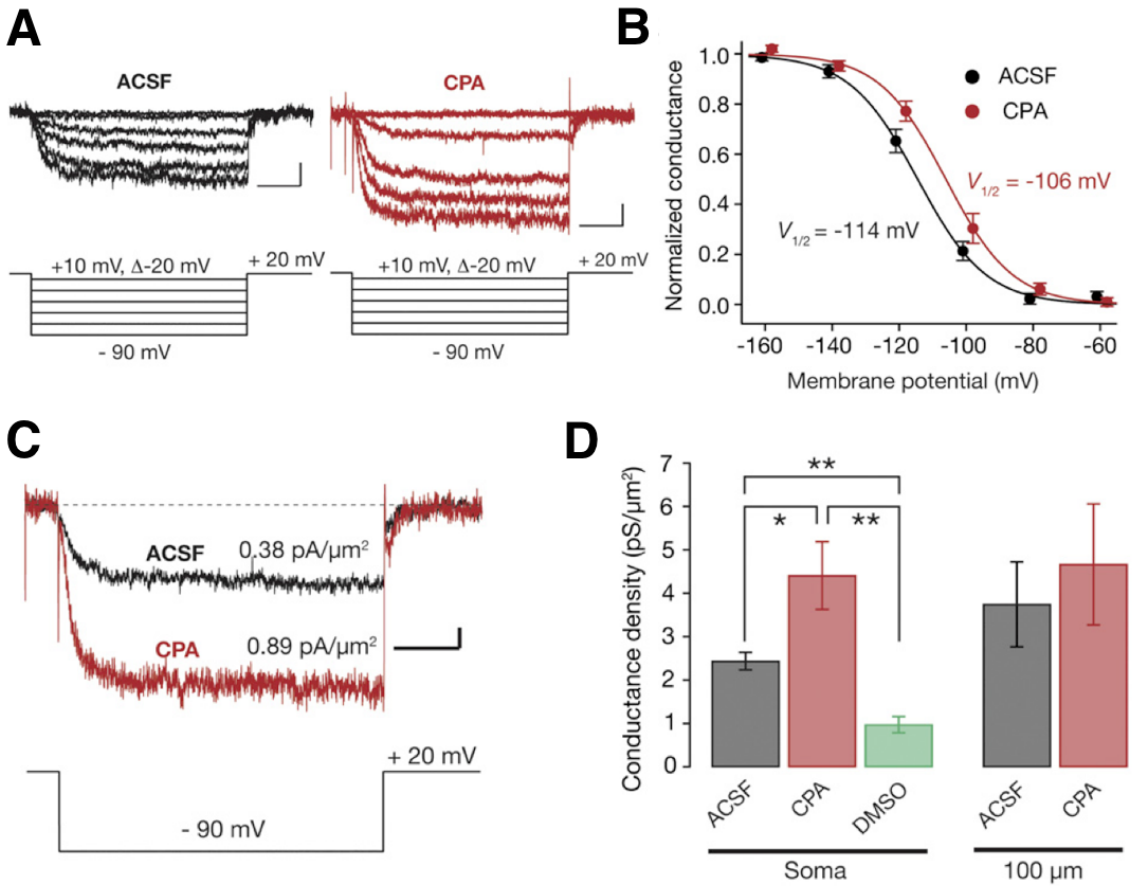

Figure 11: Effect of store depletion on the *h* current in CA1 neurons

Cell-attached voltage clamp recordings from the soma and dendrites of CA1 neurons showed a depolarizing shift in activation (A,B) and an increased conductance density of I_h (C,D). Patches made 100 µm from the soma showed no change in conductance density, suggesting that the location of plasticity was peri-somatic (D) (Narayanan et al., 2010a).

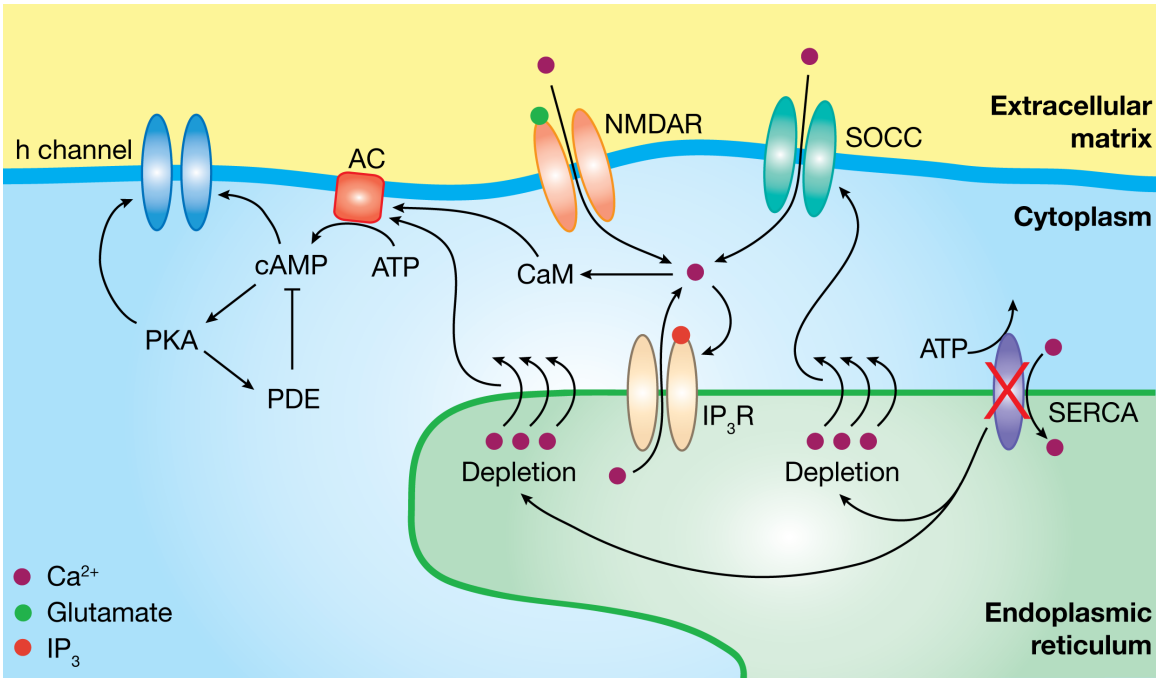

Figure 12: Mechanism of store depletion *h* plasticity

Narayanan et al. (2010) found that SD *h* plasticity was dependent on Ca^{2+} release through inositol 1,4,5 trisphosphate receptors (InsP3Rs), SOC entry and activation of protein kinase A (PKA). Figure courtesy of Rishi Narayanan, Ph.D.

V. Rationale for examining SD *h* plasticity in other age groups and hippocampal regions

Two main lines of evidence support the rationale for further examining SD *h* plasticity in other age groups and hippocampal regions.

First: SD *h* plasticity has thus far only been examined in neurons from the middle hippocampus. In addition to known behavioral differences across the longitudinal axis of the hippocampus (Moser et al., 1995; Fanselow and Dong, 2010), it is known that the dorsal and ventral (posterior and anterior in humans) hippocampus also differ in susceptibility to stress and diseases such as epilepsy, depression and anxiety (Bannerman et al., 2004). Recent work has also shown that the conductance levels, kinetics and subunit composition of *h* channels differ between dorsal and ventral neurons (Dougherty et al., 2012; Marcelin et al., 2012; Dougherty et al., 2013).

Second: Another store depletion initiated process, the UPR undergoes age-dependent modification (Naidoo, 2009; Brown and Naidoo, 2012). ER dysfunction is also associated with numerous events that are known to differentially affect the brain in adolescence and adulthood including epilepsy, sleep deprivation, stress and alcohol exposure (Holmes, 1997; Markwiese et al., 1998; Varlinskaya and Spear, 2008; Novati et al., 2011), raising the question of

whether the SD *h* plasticity in adolescent animals is mature in form or if the adult form of SD *h* plasticity is different.

Chapter 2: Materials and Methods

I. Animals

Adolescent (6.75 ± 0.19 weeks of age, *n*=22) and adult (42.15 ± 3.12 weeks of age, *n*=39) male Sprague Dawley rats were used in this study. Animals were given food and water *ad libitum* and only group-housed animals were used. All procedures were performed in accordance with the rules and regulations set forth by the University of Texas at Austin Institutional Animal Care and Use Committee.

II. Hippocampal slice preparation

Transverse slices (350 μm thick) were obtained from the dorsal and ventral hippocampal regions using isolation methods described previously (Fig. 13) (Dougherty et al., 2012). Animals were anaesthetized with an intraperitoneal injection of a combination of ketamine and xylazine and transcardially perfused with ice cold cutting saline composed of (in mM): 210 sucrose, 1.25 NaH_2PO_4, 25 $NaHCO_3$, 0.5 $CaCl_2$, 7 $MgCl_2$, 7 dextrose, 1.3 ascorbic acid, 3 sodium pyruvate, bubbled with 95%O_2/5%CO_2. Slices were transferred to a warmed (~35ºC) holding chamber containing (in mM): 125 NaCl, 2.5 KCl, 1.25 NaH_2PO_4, 25 $NaHCO_3$, 2 $CaCl_2$, 2 $MgCl_2$, 7 dextrose, 1.3 ascorbic acid, 3 sodium pyruvate,

continuously bubbled with 95%O_2/5%CO_2 and allowed to incubate for 15 min. Slices were then removed from incubation and allowed to rest at room temperature for at least 45 min prior to recording. For most animals, one hemisphere was used to obtain dorsal slices and the other for ventral slices. The hemisphere (left or right) used for dorsal or ventral slices was alternated daily.

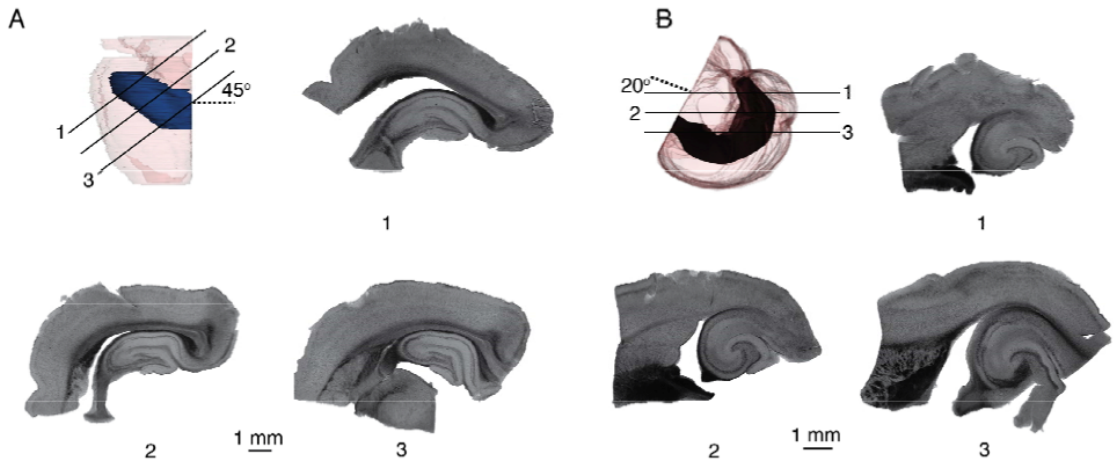

Figure 13: Preparation of dorsal and ventral hippocampal slices

(A) Illustration of blocking cuts used to extract transverse slices from the dorsal hippocampus. Three examples of dorsal hippocampal slices are shown. (B) Illustration of blocking cuts used to extract transverse slices from the ventral hippocampus. Three examples of ventral hippocampal slices are shown (Dougherty et al., 2012).

III. Electrophysiology

Whole-cell patch clamp recordings in current-clamp mode were made from the soma or the dendrites of CA1 pyramidal neurons using a Dagan BVC-700 (Dagan Corp, Minneapolis, Minnesota) amplifier. Signals were low-pass filtered at 5 kHz and sampled at 10–30 kHz. Recordings were made at ~34º C and slices were constantly perfused with external recording solution (in mM): 125 NaCl, 3 KCl, 1.25 NaH_2PO_4, 25 $NaHCO_3$, 2 $CaCl_2$, 1 $MgCl_2$, 12.5 dextrose, continuously bubbled with 95%O_2/5%CO_2. A 5–20 ms hyperpolarizing current injection (300–500 pA) was used to monitor changes in series resistance. Experiments were discarded if the series resistance exceeded 35 MΩ. Data acquisition and analysis were performed with custom-written software in IGOR Pro (Wavemetrics Inc., USA) that controlled an Instrutech ITC-18 (Heka, Bellmore, New York) data acquisition module. All experiments were performed in the presence of the synaptic blockers 20 µM DNQX and 2 µM gabazine. Electrodes were filled with an internal solution of the following composition (in mM): 120 K-gluconate, 20 KCl, 10 HEPES, 4 NaCl, 4 Mg-ATP, 0.3 Na-GTP, 7 K_2-phosphocreatine, pH = 7.37 adjusted with KOH. Voltages were not corrected for the liquid junction potential (~8 mV).

IV. Measurements

Input resistance (R_{in}) was measured as the slope of a linear fit to the steady state *V–I* plot obtained by injecting subthreshold, 500 ms-duration current pulses of amplitudes spanning –50 pA to 50 pA, in steps of 10 pA. Stimulus used for characterizing impedance parameters was a sinusoidal current of constant amplitude, a *Chirp* stimulus, with its frequency linearly spanning 0–15 Hz in 15 s. The frequency at which the impedance amplitude reached its maximum was the resonance frequency (f_R).

V. Neuron inclusion criteria and histological processing

Prior to electrophysiological recording, neurons were visualized with differential interference contrast (DIC) microscopy using a Zeiss Axioskop 2 microscope fitted with a 40X or 63X (Zeiss) water-immersion objective. Cells located in the center of the CA1 cell body layer (equidistant from the CA2 and subiculum in the transverse axis) were targeted for patching.

Neurobiotin (Vector Laboratories, Burlingame, CA) was included in the patch pipette solution (0.1—0.2%) to allow for post-hoc visualization of neuronal location and morphology. Slices were fixed in a 3% glutaraldehyde solution (prepared in 0.1 M phosphate buffer, pH 7.4) and stored at 4°C before

undergoing histological processing. Processing was performed using an avidin-HRP system activated by diaminobenzidine (DAB; Vector Laboratories, Burlingame, CA). Processed slices were mounted in glycerol and visualized with a compound (Leitz Diaplan) microscope. Inclusion criteria for neuronal morphology and location are similar to those used in (Dougherty et al., 2012). This included a confirmation that the neuron maintained a robust apical and basal dendritic arbor and also that the location of the soma in the transverse axis was contained within the CA1 and did not extend into CA2 or subicular layers. This second criterion was particularly important in the case of VHC slices, which have a relatively short CA1 cell body layer.

VI. Drugs and chemicals

Most extracellular solution salts were procured from Fisher Scientific. $CaCl_2$, K–Gluconate, MgATP, NaGTP, sucrose, ascorbic acid, and sodium pyruvate were from Sigma-Aldrich. HEPES, and K_2Phosphocreatine were from EMD Millipore. CPA and ZD7288 were from Abcam Biochemicals. Nimodipine was from Tocris Bioscience. Appropriate controls were performed for each of the drugs used in order to ensure that no time dependent changes were initiated by just the presence of the drug in the bath or the pipette.

VII. Statistical analysis

Group data are expressed as the mean ± standard error of the mean. Statistical significance was calculated using unpaired or paired *Student's t* tests. Wilcoxon's Ranked Sum (RS) test was applied when *n* was less than 7 or when the variances were unequal. Hypothesis testing was performed with $\alpha = 0.05$.

Chapter 3: Results

I. Differences in intrinsic properties between dorsal and ventral hippocampal neurons from adolescent animals

To examine differences in the basic intrinsic properties of CA1 pyramidal neurons from the adolescent hippocampus, measures of excitability and resonance were examined using whole cell patch clamp recordings from somata of dorsal (DHC) and ventral (VHC) neurons. Resting membrane potential (RMP) was more depolarized for VHC neurons (DHC: –64.50 ± 0.87 mV; VHC: –62.88 ± 1.01 mV) and input resistance was higher for VHC neurons (DHC: 66.21 ± 7.39 MΩ; VHC: 89.04 ± 7.35 MΩ) (Fig. 14). Based on these two measures, VHC neurons can be considered to be more excitable than DHC neurons. Resonant properties of adolescent DHC and VHC neurons were also examined (Fig. 15). VHC neurons had significantly higher resonant frequencies compared with DHC neurons (DHC: 3.39 ± 0.14 Hz; VHC: 4.51 ± 0.26 Hz). These results confirmed that DHC and VHC neurons from adolescent animals have significantly different levels of excitability and frequency response properties, which is in agreement with previous work from our lab and others.

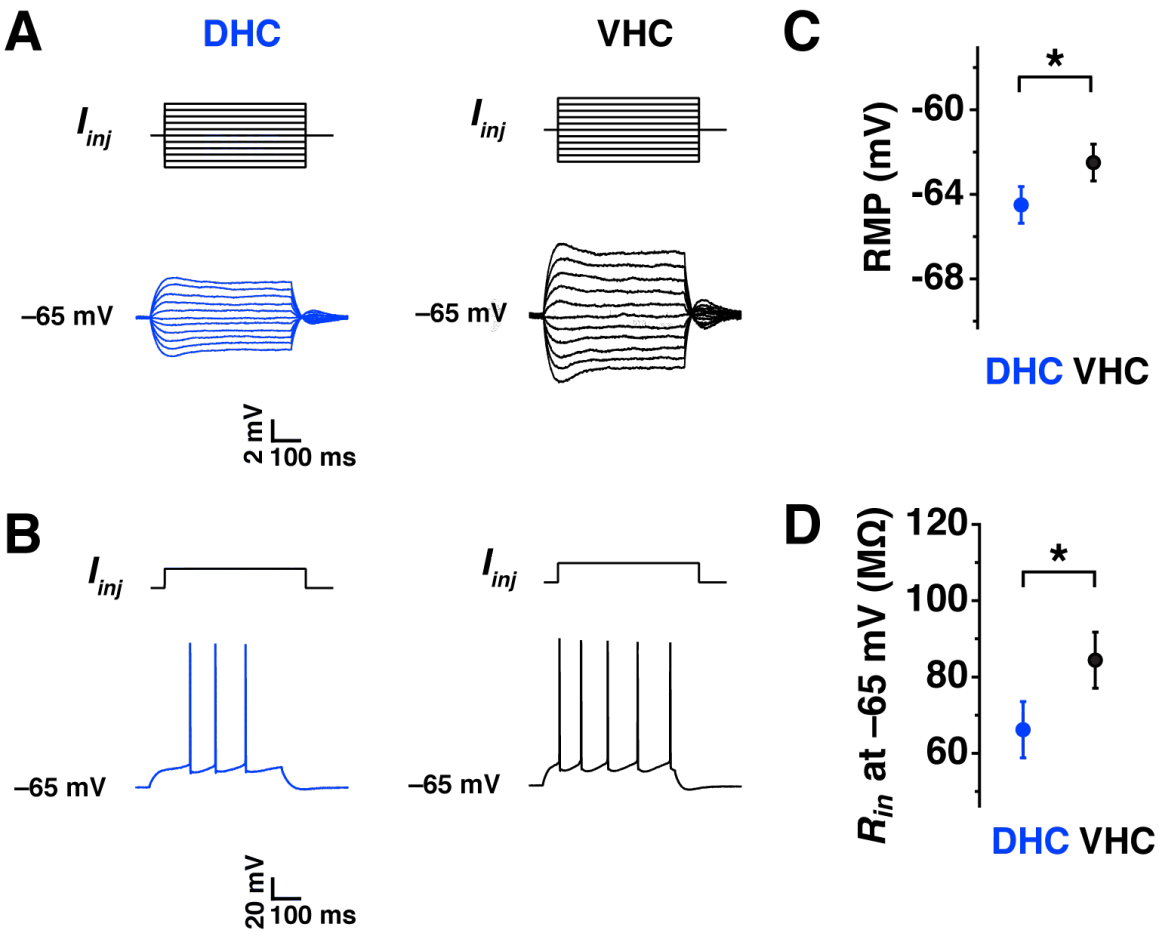

Figure 14: Ventral hippocampal neurons are more excitable than dorsal hippocampal neurons from adolescent animals.

(A) Representative traces used for measurement of input resistance (R_{in}) in DHC and VHC neurons. Current steps range from –50 pA to +50 pA in 10 pA increments. (B) Example spiking pattern for DHC and VHC neurons for a 150 pA current injection. (C) Average resting membrane potential (RMP) for DHC and VHC neurons. Error bars are standard error of the mean (S.E.M.) (D) Average input resistance (R_{in}) measurements for DHC and VHC neurons. Error bars are standard error of the mean (S.E.M.).

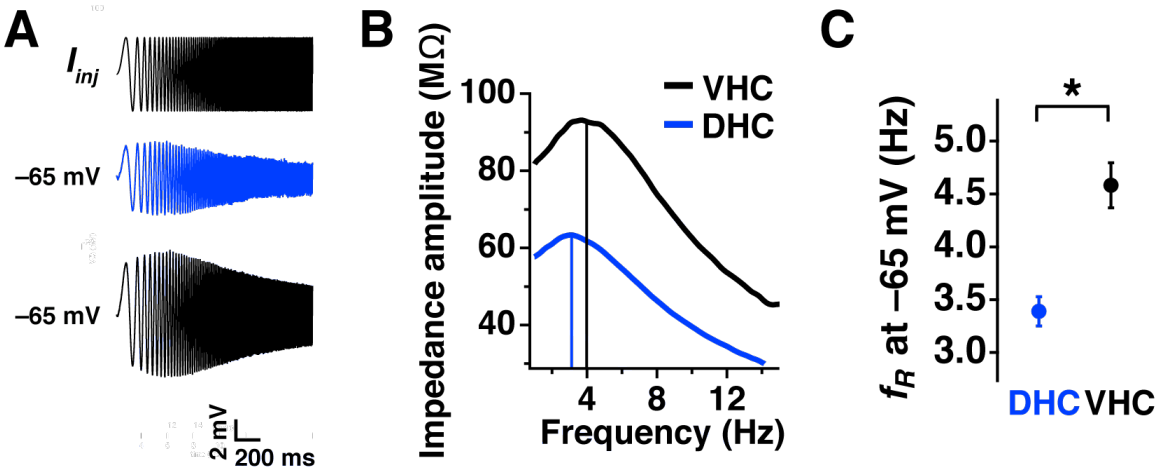

Figure 15: Ventral hippocampal neurons have higher resonance frequencies when compared with dorsal hippocampal neurons from adolescent animals.

(A) Representative traces used for measurement of resonance frequency (f_R) in DHC (blue) and VHC (black) neurons. (B) Impedance profiles for representative DHC and VHC neurons. (C) Average resonance frequency for DHC and VHC neurons. Error bars are standard error of the mean (S.E.M.).

II. Experimental protocol for store depletion *h* plasticity

The experimental protocol used for induction of store depletion (SD) *h* plasticity was identical to that used in Narayanan et al. (2010). Data from a representative adolescent VHC cell are shown here for illustrative purposes (Fig. 16). After obtaining whole-cell current clamp configuration, the recording was allowed to stabilize for a few min and the resting membrane potential (RMP) of the cell was noted (Fig. 16A). Following the stabilization period, current was injected to hold the cell at –65 mV in order to make the before CPA measurements of input resistance (R_{in}) and resonance frequency (f_R). Next, the cell was returned to its RMP (I_{inj}=0 pA) and a current stimulus consisting of a short –50 pA current step and a chirp stimulus (Fig. 16A, top right), was given once every 30–60 s to give estimates of R_{in} and f_R. Following a baseline period of 5 min, 20 μM CPA was applied for 10 min. In some cases, cells depolarized from their RMP. In these cases, a holding current was applied to maintain the initial RMP. After application of CPA, the R_{in} gradually decreased and f_R increased. After monitoring the change in R_{in} and f_R for 30—40 min, a holding current was again applied to hold the cell at –65 mV for after CPA measurement of R_{in} and f_R. A comparison of the before CPA and after CPA measurements at –65 mV are shown in Figure 16B,C.

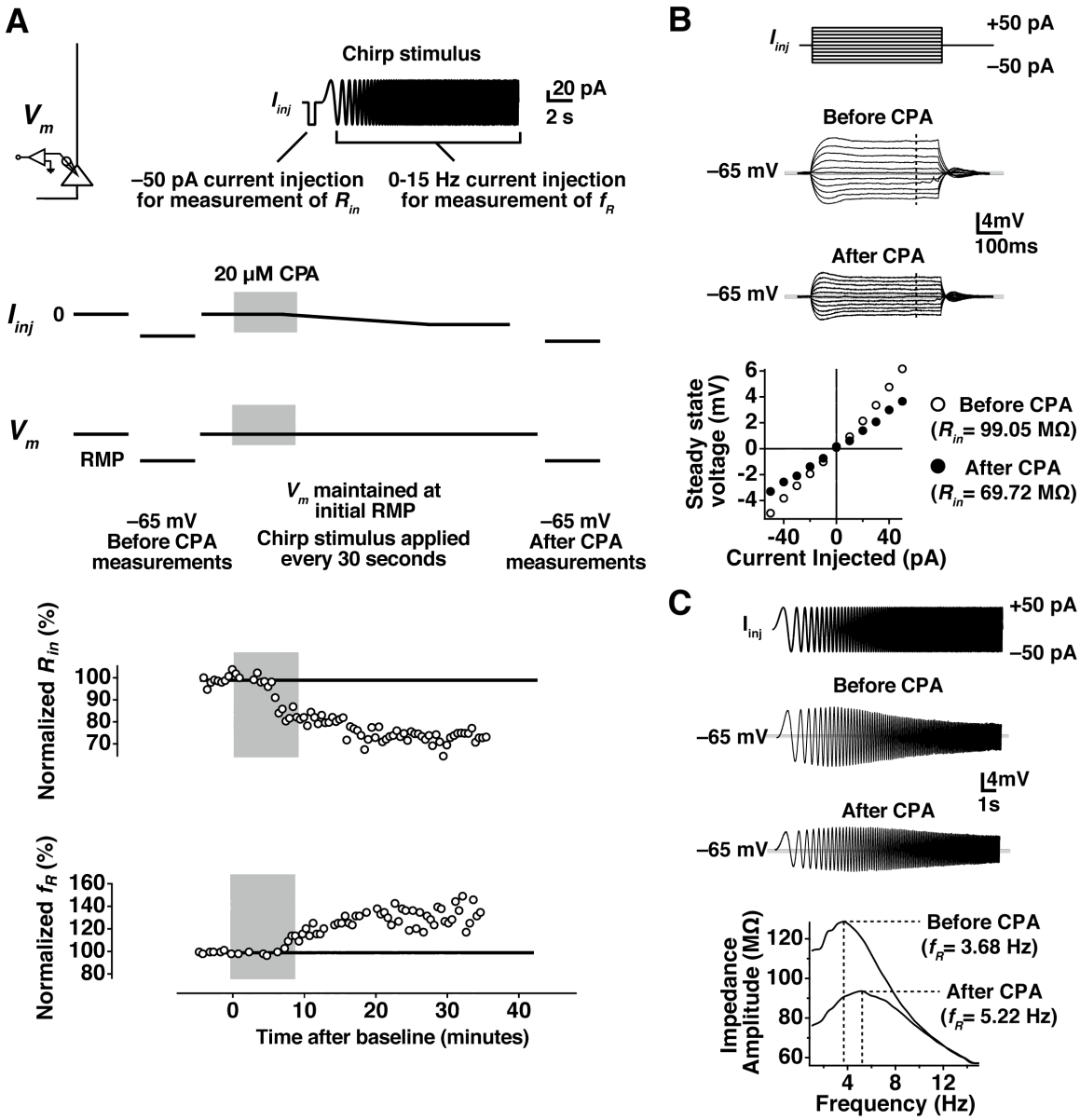
A
Chirp stimulus
I_{inj}
20 pA
2 s
V_m
–50 pA current injection for measurement of R_{in}
0-15 Hz current injection for measurement of f_R
20 µM CPA
I_{inj} 0
V_m
RMP
V_m maintained at initial RMP
Chirp stimulus applied every 30 seconds
–65 mV Before CPA measurements
–65 mV After CPA measurements
Normalized R_{in} (%)
100
90
80
70
Normalized f_R (%)
160
140
120
100
80
0
10
20
30
40
Time after baseline (minutes)
B
I_{inj}
+50 pA
–50 pA
Before CPA
–65 mV
4mV
100ms
After CPA
–65 mV
Steady state voltage (mV)
6
4
2
0
-2
-4
-40
0
40
Current Injected (pA)
Before CPA (R_{in}= 99.05 MΩ)
After CPA (R_{in}= 69.72 MΩ)
C
I_{inj}
+50 pA
–50 pA
Before CPA
–65 mV
4mV
1s
After CPA
–65 mV
Impedance Amplitude (MΩ)
120
100
80
60
4
8
12
Frequency (Hz)
Before CPA (f_R= 3.68 Hz)
After CPA (f_R= 5.22 Hz)

Figure 16: Experimental protocol for induction of SD *h* plasticity

(A) After obtaining the whole-cell recording configuration (upper left), the neuron was allowed to stabilize and the resting membrane potential (RMP, with 0 current injection) was noted. Current was then injected (I_{inj}) to hold the cell at –65 mV and before CPA measurements of R_{in} and f_R were made. The cell was then returned to its RMP and the chirp stimulus (upper right) was applied to measure R_{in} and f_R every 30—60 seconds. After a baseline period of 5 min, CPA was applied for 10 min. As depicted in this example, current had to be injected to maintain the membrane potential at the initial RMP. Following 40–60 min of recording after the baseline measurements, current was again injected to hold cells at –65 mV for the after CPA measurement of R_{in} and f_R. A representative time course for change in the normalized R_{in} and normalized f_R are shown. (B) Current steps from –50 pA to +50 pA in 10 pA steps were applied to measure R_{in} during the before CPA and after CPA periods. Voltage deflections for the current steps are shown before and after for this cell. The slope in the steady-state voltage deflection vs. amplitude of current injection was taken in each case, giving the input resistance. (C) A chirp stimulus was given during the before CPA and after CPA measurement period to estimate resonance frequency at –65 mV. Voltage responses before and after CPA are depicted. The resonance frequency (f_R) was obtained from the transformation of these voltage responses to the frequency domain (bottom). The frequency at which the largest impedance was seen (f_R) increased in this representative example.

II. Store depletion *h* plasticity is observed at the somata of dorsal and ventral neurons from adolescent animals.

SD *h* plasticity was first characterized in neurons from the middle hippocampus from adolescent (4–9 week old) animals (Narayanan et al., 2010b). Given the significant differences in *h* channel composition, intrinsic properties and synaptic plasticity across the dorso-ventral axis of the hippocampus (Dougherty et al., 2012; Grigoryan et al., 2012; Marcelin et al., 2012; Dougherty et al., 2013), the question arose, whether DHC and VHC neurons from adolescents differ in their response to store depletion. Each neuron was maintained at its initial RMP for the induction of store depletion plasticity while R_{in} and f_R were measured once every 30–60 s. The average initial RMPs for DHC and VHC neurons are displayed in part A of Fig. 17,18 as blue and black lines, respectively (DHC: –64.50 ± 0.87 mV; VHC: –62.88 ± 1.01 mV). R_{in} and f_R were measured before and 30–40 min after CPA at –65 mV.

The change in R_{in} over time for DHC and VHC neurons is shown in Figure 17B. R_{in} was significantly reduced when measured at –65 mV after CPA for DHC (Fig. 17C,D; Appendix, Table 1; before CPA: 66.21 ± 7.39 MΩ; after CPA: 49.52 ± 9.03 MΩ; $p < 0.05$) and VHC neurons (Fig. 17C,D; Appendix, Table 1; before CPA: 89.04 ± 7.35 MΩ; after CPA: 66.62 ± 5.01 MΩ; $p < 0.05$). The change in f_R over time for DHC and VHC neurons is shown in Figure 18B. f_R was significantly increased when measured at –65 mV after CPA for DHC (Fig. 18C,D; Appendix,

Table 1; before CPA: 3.39 ± 0.14 Hz; after CPA: 4.11 ± 0.15 Hz; $p < 0.05$) and VHC neurons (Fig. 18C,D; Appendix, Table 1; before CPA: 4.51 ± 0.26 Hz; after CPA: 5.80 ± 0.49 Hz; $p < 0.05$).

In Fig. 19 these results are summarized. The percent reduction in R_{in} and f_R was proportional for DHC and VHC neurons over time (Fig. 19A) even though the initial values of R_{in} and f_R differed between DHC and VHC neurons. The percentage change in R_{in} and f_R measured from –65 mV were also similar between adolescent DHC (percent reduction in R_{in}: 26.76 ± 4.71; percent increase in f_R: 21.47 ± 5.12) and VHC neurons (percent reduction in R_{in}: 24.73 ± 4.39; percent increase in f_R: 28.37 ± 6.14). Thus, although DHC and VHC neurons from adolescent animals start with different intrinsic properties, they respond to store depletion with similar percentage changes in R_{in} and f_R.

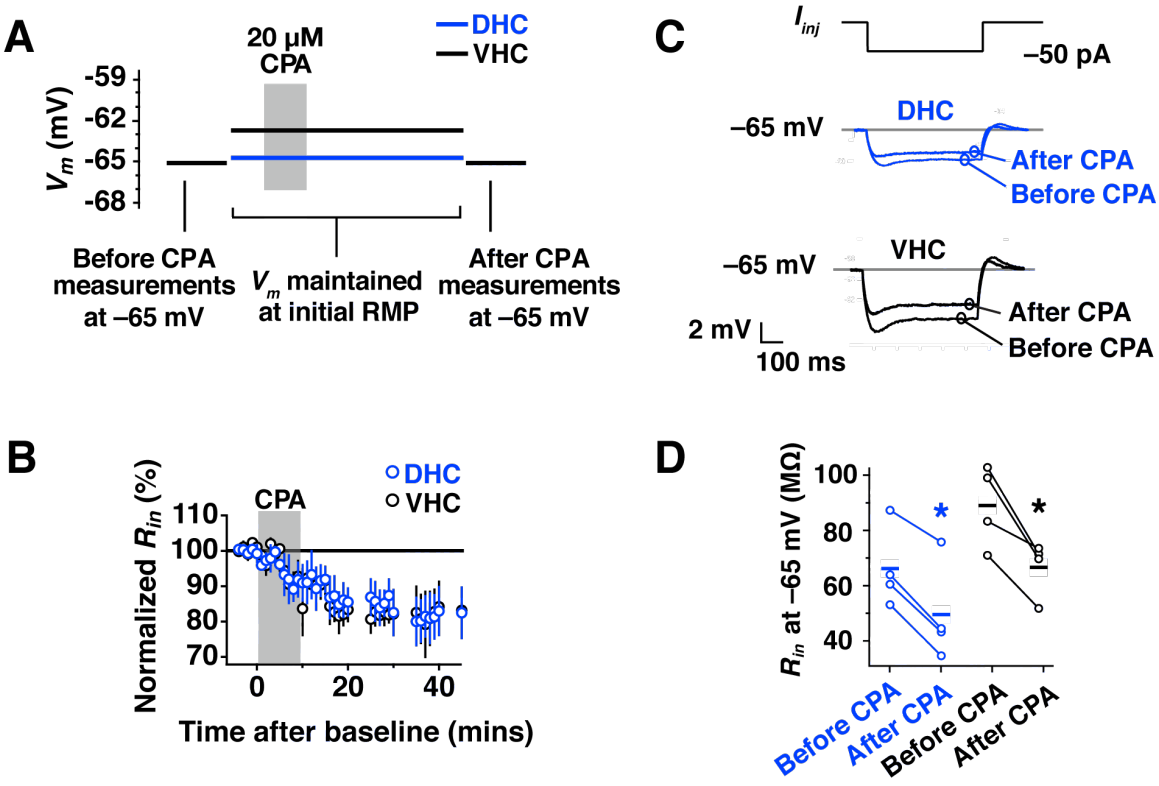

Figure 17: Input resistance changes with SD *h* plasticity in dorsal and ventral hippocampal neurons from adolescent animals.

(A) Voltages used in each portion of the plasticity experiment. Before CPA measures were made at –65 mV. Neurons were then returned to their resting membrane potential (RMP) and maintained there for the subsequent 40—60 minute recording period. Black and blue lines indicate average initial RMP values for VHC and DHC neurons, respectively. Neurons were again held at –65 mV at the end of the experiment to collect after CPA measurements. (B) The time course of change in normalized R_{in} for DHC and VHC neurons. (C) Representative before CPA and after CPA traces for the measurement of R_{in}. Voltage traces shown are responses to a –50 pA current injection. (D) Before and after CPA measurements of R_{in} (at –65 mV) for all cells. Horizontal bars indicate average values and stars indicate a significant reduction in R_{in} with a paired statistical test ($p < 0.05$).

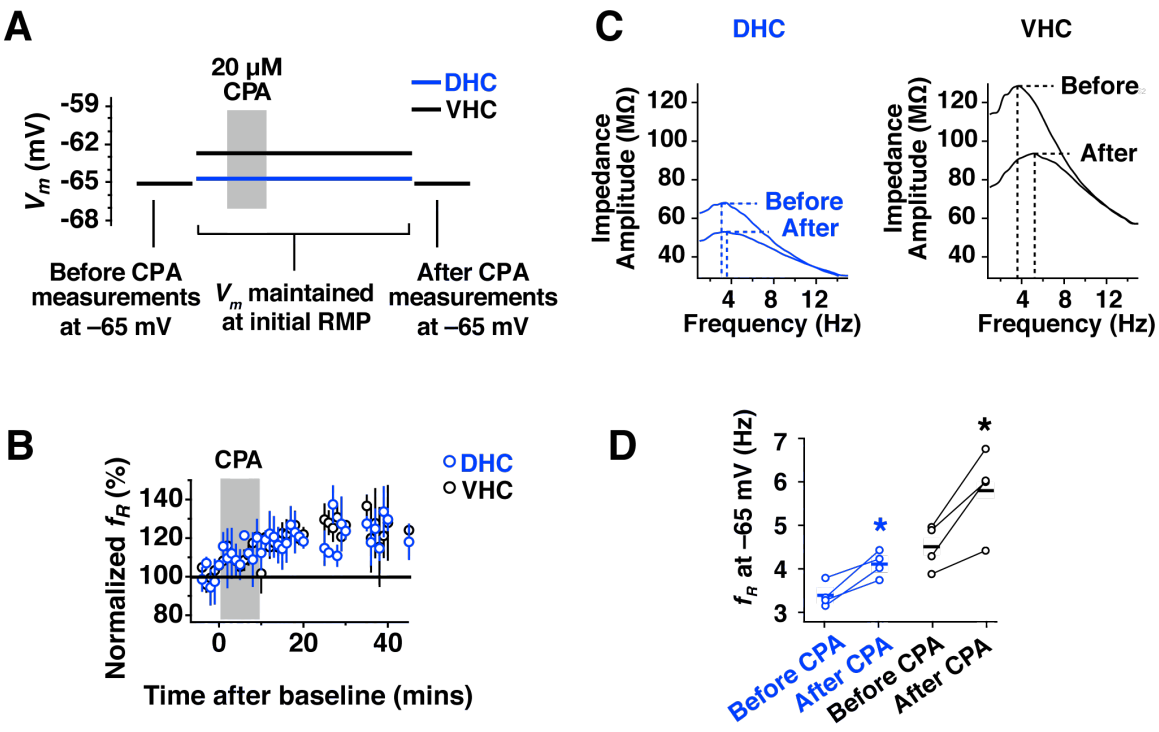

Figure 18: Resonance frequency changes with SD *h* plasticity in dorsal and ventral hippocampal neurons from adolescent animals.

(A) Voltages used in each portion of the plasticity experiment. Before CPA measures were made at –65 mV. Neurons were then returned to their resting membrane potential (RMP) and maintained there for the subsequent 40—60 minute recording period. Black and blue lines indicate average initial RMP values for VHC and DHC neurons, respectively. Neurons were again held at –65 mV at the end of the experiment to collect after CPA measurements. (B) The time course of change in normalized f_R for DHC and VHC neurons. (C) Representative before and after CPA impedance traces (performed at –65 mV). (D) Before and after CPA measurements of f_R (at –65 mV). Horizontal bars indicate average values and stars indicate a significant increase in f_R with a paired statistical test ($p < 0.05$).

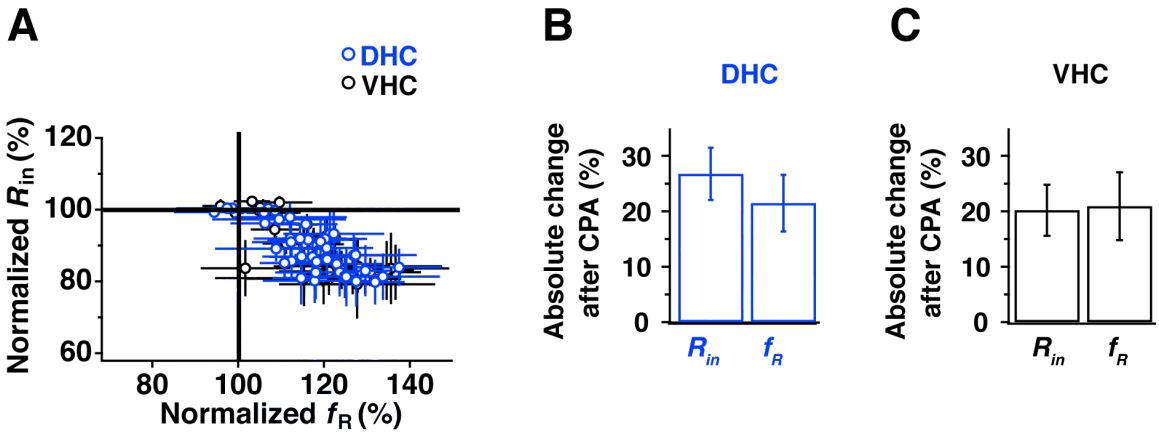

Figure 19: Summary of changes with SD *h* plasticity in dorsal and ventral neurons from adolescent animals

(A) Normalized change in R_{in} vs. normalized change in f_R that were observed over time. Absolute changes in percent R_{in} and f_R for DHC (B) and VHC (C) neurons.

I. Differences in intrinsic properties between dorsal and ventral hippocampal neurons from adult animals

Before examining SD *h* plasticity in adult animals, the basic intrinsic properties in adult DHC and VHC neurons were measured. No change was observed in RMP, R_{in} or f_R when adult DHC and VHC neurons were compared with adolescent neurons (Fig. 20). Similar to what was observed for neurons from adolescent animals, in neurons from adult animals: RMP was more depolarized for VHC neurons (Fig. 20C; DHC: –65.90 ± 1.01 mV; VHC: –63.83 ± 0.69 mV); input resistance was higher for VHC neurons (Fig. 20D; DHC: 59.59 ± 2.52 MΩ; VHC: 81.94 ± 3.46 MΩ); and resonance frequency was higher for adult neurons (Fig. 20E; DHC: 3.49 ± 0.14 Hz; VHC: 3.95 ± 0.17 Hz).

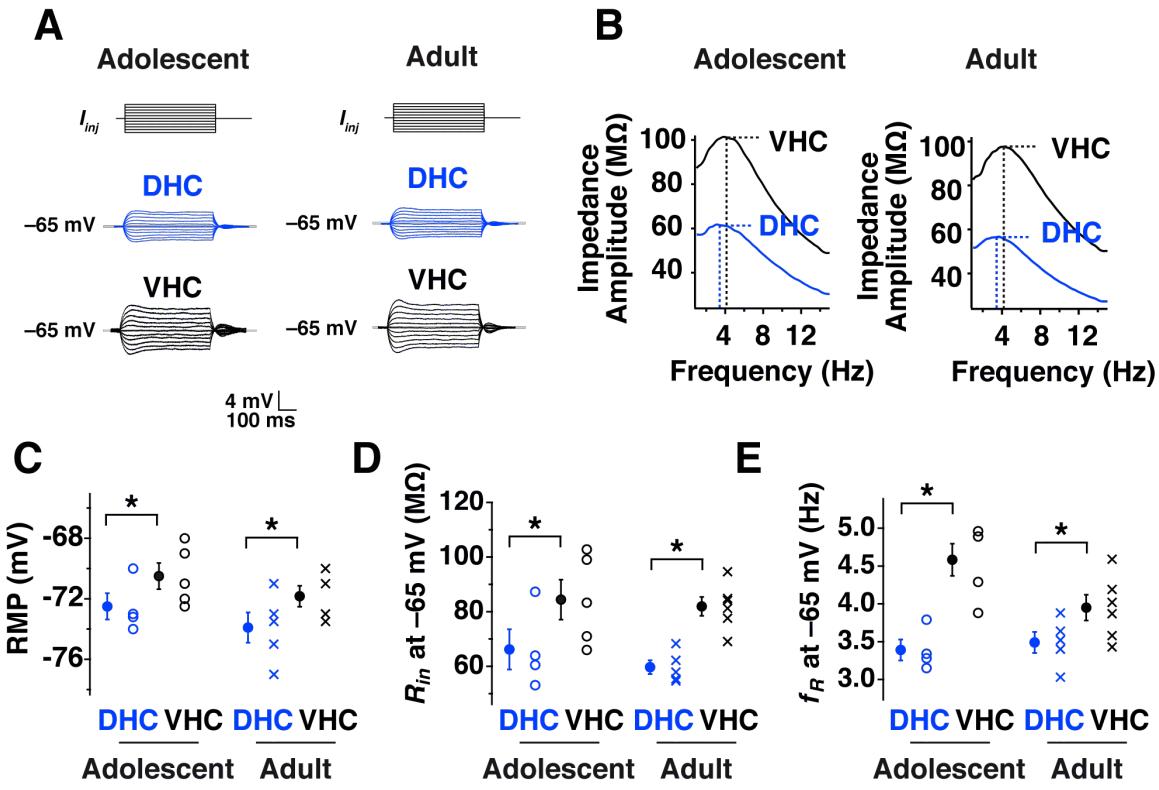

Figure 20: Intrinsic properties for adolescent and adult dorsal and ventral neurons

(A) Representative traces used for measurement of input resistance (R_{in}) in DHC and VHC neurons. Current steps range from –50 pA to +50 pA in 10 pA increments. (B) Impedance profiles for representative DHC and VHC neurons. (C) Average resting membrane potential (RMP) for DHC and VHC neurons. Error bars are standard error of the mean (S.E.M.) (D) Average input resistance (R_{in}) measurements for DHC and VHC neurons. Error bars are standard error of the mean (S.E.M.). (E) Average resonance frequency for DHC and VHC neurons. Error bars are standard error of the mean (S.E.M.).

III. Store depletion *h* plasticity is observed at the somata of ventral but not dorsal neurons from adult animals.

To address the possible age-dependence of SD *h* plasticity, experiments were performed in DHC and VHC neurons from adult animals. SD *h* plasticity was performed at the initial resting potential for adult DHC and VHC neurons (Fig. 21,22A; Appendix, Table 2; DHC: –65.90 ± 1.07 mV; VHC: –63.83 ± 0.69 mV). The change in R_{in} over time for DHC and VHC neurons is shown in Figure 21B. In DHC neurons, R_{in} was not significantly changed when measured at –65 mV (Fig. 21C,D; Appendix, Table 2; before CPA: 59.59 ± 2.52 MΩ; after CPA: 57.76 ± 2.82 MΩ; $p > 0.05$) though R_{in} was reduced for VHC neurons (Fig. 21C,D; Appendix, Table 2; before CPA: 81.94 ± 3.46 MΩ; after CPA: 58.00 ± 3.25 MΩ; $p < 0.05$). The change in f_R over time for DHC and VHC neurons is shown in Figure 22B. No change in f_R was seen when measured at –65 mV for DHC neurons (Fig. 22C,D; Appendix, Table 2; before CPA: 3.49 ± 0.14 Hz; after CPA: 3.66 ± 0.24 Hz; $p > 0.05$) though a significant increase was observed for VHC neurons (Fig. 22C,D; Appendix, Table 2; before CPA: 3.95 ± 0.17 Hz; after CPA: 4.40 ± 0.36 Hz; $p < 0.05$).

In Fig. 23 these results are summarized. The percent reduction in R_{in} and f_R over time hovered around zero for DHC neurons and for VHC neurons, the percent reduction in R_{in} was not proportional to the increase in f_R. In Fig. 23B,C the percentage change in R_{in} and f_R are shown for neurons from the adult DHC

(percent reduction in R_{in}: 3.13 ± 3.38; percent increase in f_R: 4.58 ± 3.57) and VHC (percent reduction in R_{in}: 28.23 ± 5.82; percent increase in f_R: 10.60 ± 4.50).

The observed measures of plasticity for DHC neurons were significantly different when compared across the two ages (Fig. 24); the reduction in R_{in} (adolescent decrease in R_{in} after CPA: 16.69 ± 1.78 MΩ; adult decrease in R_{in} after CPA: 1.93 ± 2.00 MΩ; $p < 0.0005$) and increase in f_R (adolescent increase in f_R after CPA: 0.72 ± 0.16 Hz; adult increase in f_R after CPA: 0.17 ± 0.14 Hz; $p < 0.05$) were both reduced for adult animals. For VHC neurons, however, there was no age-dependent change in the reduction of R_{in} after CPA (adolescent decrease in R_{in} after CPA: 22.42 ± 4.98 MΩ; adult decrease in R_{in} after CPA: 23.94 ± 5.63 MΩ; $p > 0.05$), though there was an age-dependent reduction in the increase of f_R (adolescent increase in f_R after CPA: 1.30 ± 0.30 Hz; adult increase in f_R after CPA: 0.45 ± 0.20 Hz; $p < 0.05$).

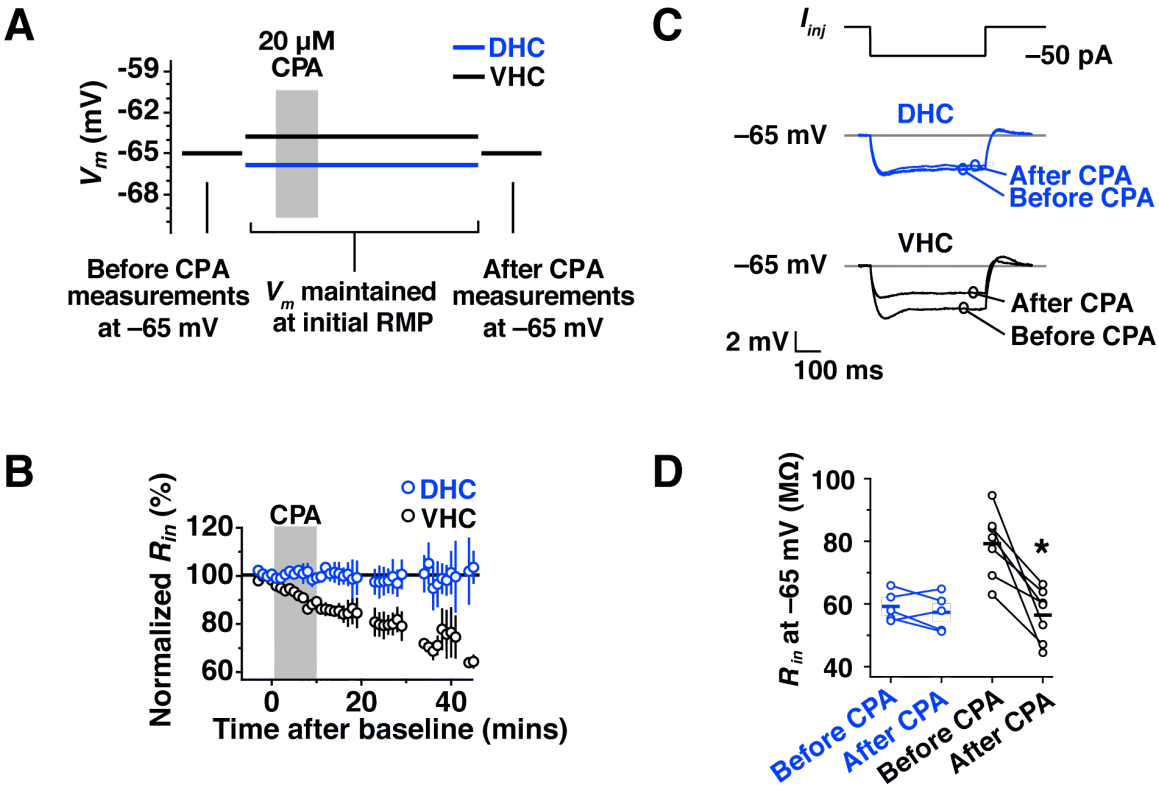

Figure 21: Input resistance changes with SD *h* plasticity in dorsal and ventral hippocampal neurons from adult animals.

(A) Voltages used in each portion of the plasticity experiment. Before CPA measures were made at –65 mV. Neurons were then returned to their resting membrane potential (RMP) and maintained there for the subsequent 40—60 minute recording period. Black and blue lines indicate average initial RMP values for VHC and DHC neurons, respectively. Neurons were again held at –65 mV at the end of the experiment to collect after CPA measurements. (B) The time course of change in normalized R_{in} for DHC and VHC neurons. (C) Representative before CPA and after CPA traces for the measurement of R_{in}. Voltage traces shown are responses to a –50 pA current injection. (D) Before and after CPA measurements of R_{in} (at –65 mV) for all cells. Horizontal bars indicate average values and stars indicate a significant reduction in R_{in} with a paired statistical test ($p < 0.05$).

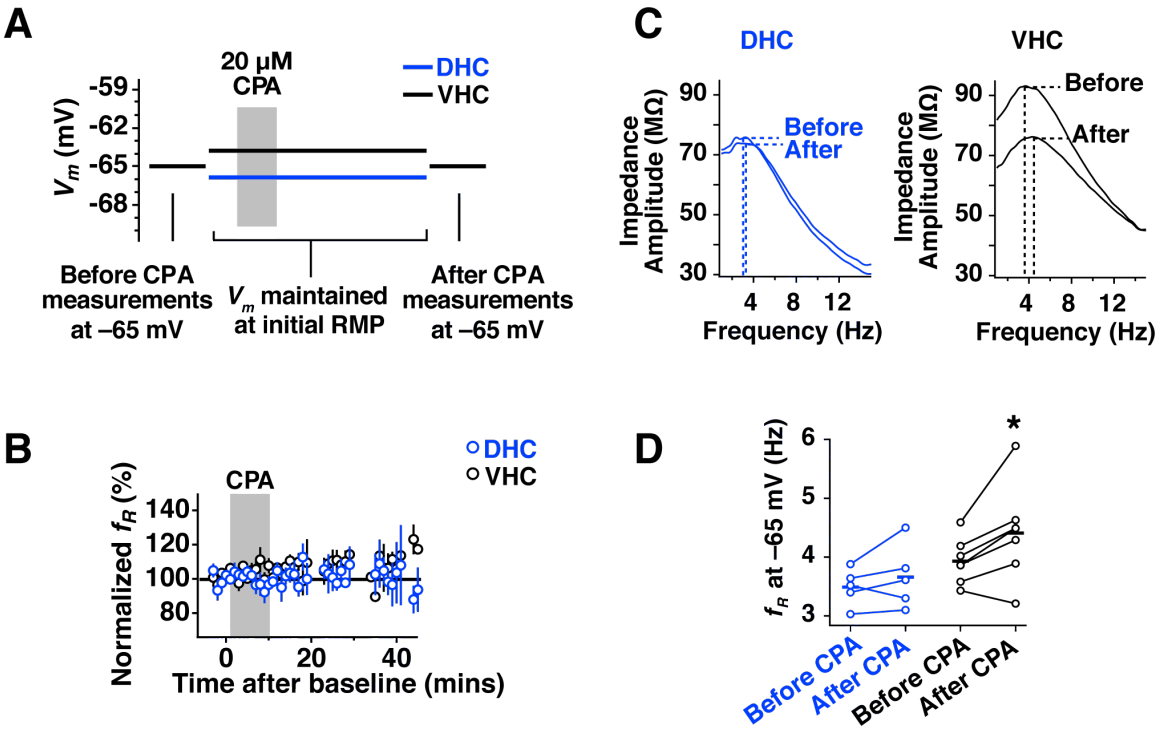

Figure 22: Resonance frequency changes with SD *h* plasticity in dorsal and ventral hippocampal neurons from adult animals.

(A) Voltages used in each portion of the plasticity experiment. Before CPA measures were made at –65 mV. Neurons were then returned to their resting membrane potential (RMP) and maintained there for the subsequent 40—60 minute recording period. Black and blue lines indicate average initial RMP values for VHC and DHC neurons, respectively. Neurons were again held at –65 mV at the end of the experiment to collect after CPA measurements. (B) The time course of change in normalized f_R for DHC and VHC neurons. (C) Representative before and after CPA impedance traces (performed at –65 mV). (D) Before and after CPA measurements of f_R (at –65 mV). Horizontal bars indicate average values and stars indicate a significant increase in f_R with a paired statistical test ($p < 0.05$).

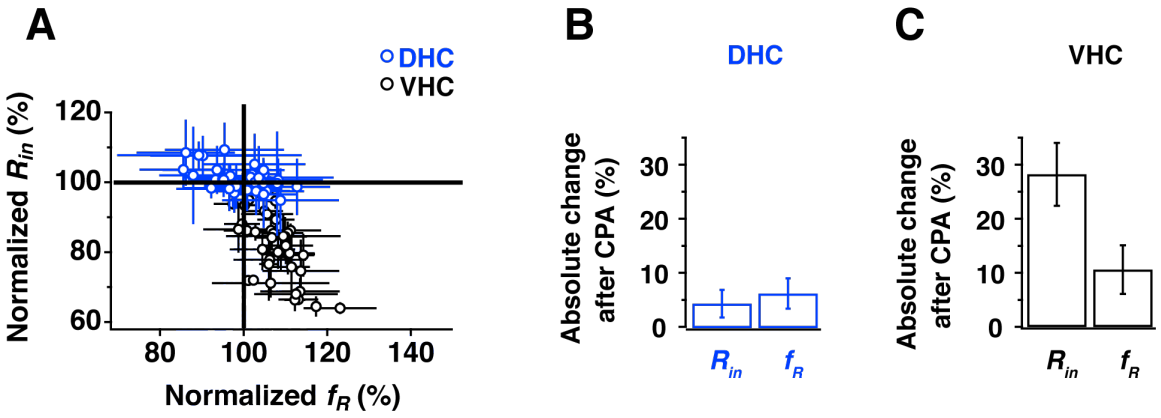

Figure 23: Summary of changes with SD *h* plasticity in dorsal and ventral neurons from adult animals

(A) Normalized change in R_{in} vs. normalized change in f_R that were observed over time. Absolute changes in percent R_{in} and f_R for DHC (B) and VHC (C) neurons.

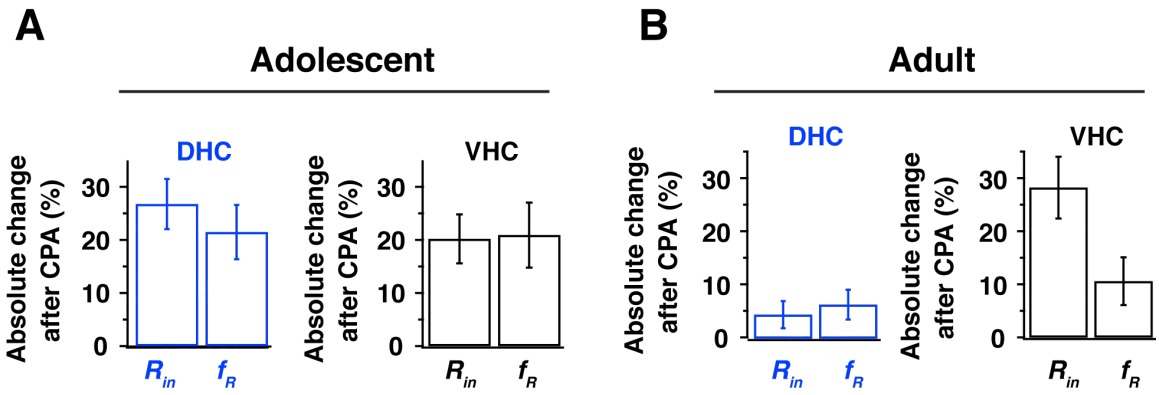

Figure 24: Summary of SD *h* plasticity induced changes for neurons from adolescent and adult animals

III. Store depletion *h* plasticity in adult animals is blocked by ZD7288.

To test the hypothesis that the modified form of plasticity observed in VHC neurons is due to a change in a current other than I_h, plasticity experiments were performed in the presence of the *h* channel blocker, ZD7288 (20 μM in the patch pipette). Control experiments showed that long-term stable recordings could be achieved in the presence of ZD7288. As expected from a blockade of HCN channels, ZD7288 produced a significant hyperpolarization of the RMP (VHC without ZD7288: –63.83 ± 0.69 mV; VHC with ZD7288: –68.20 ± 1.24 mV). For consistency in the experimental protocol, neurons in the presence of ZD7288 were maintained at the average initial RMP for a VHC neuron without ZD7288 (–63 mV; Fig. 25A). In the presence of ZD7288, no changes were observed in RMP (before CPA: –68.20 ± 1.24 mV; after CPA: –70.00 ± 1.92 mV; $p > 0.05$), R_{in} (Fig. 25B—E; before CPA: 97.09 ± 7.02 MΩ; after CPA: 102.96 ± 7.98 MΩ; $p > 0.05$) or f_R (Fig 25D,E; before CPA: 1.12 ± 0.12 Hz; after CPA: 1.00 ± 0.00 Hz; $p > 0.05$) after CPA (Appendix, Table 2), suggesting that the plasticity observed in VHC neurons from mature adult animals was mediated by a change in *h* channels.

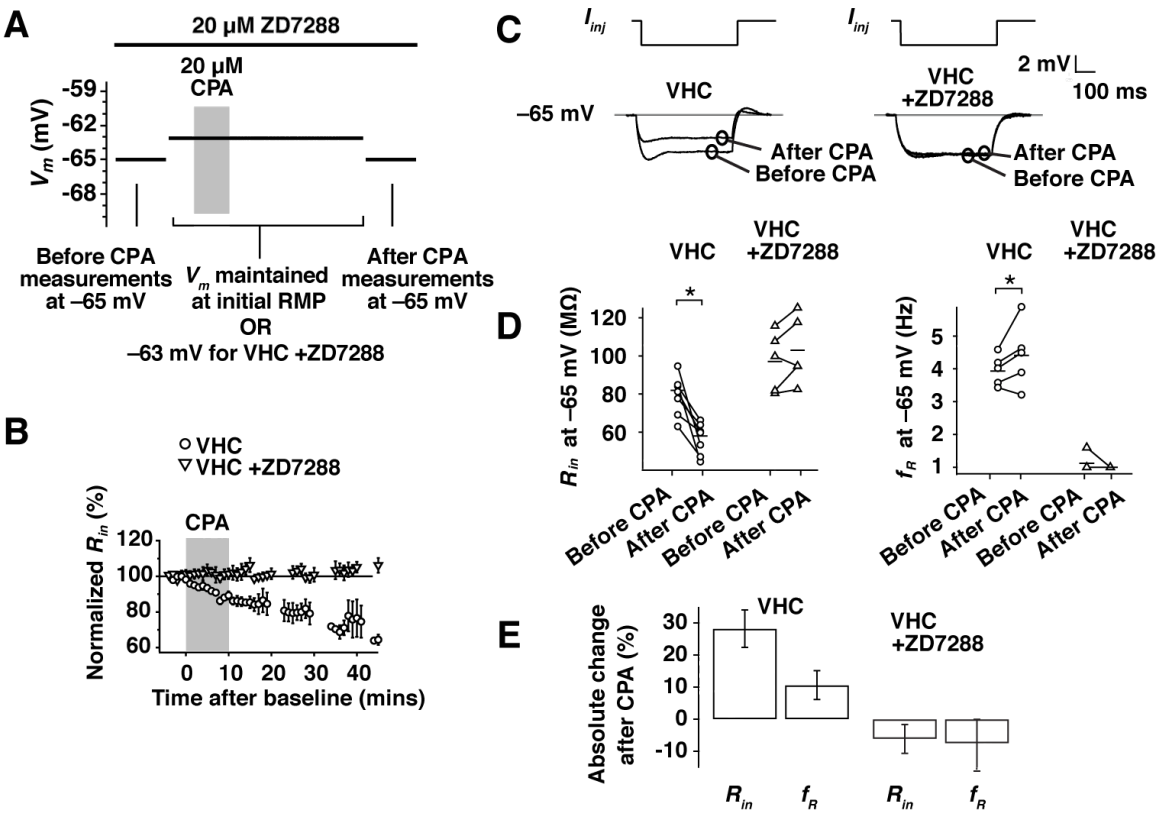

Figure 25: SD *h* plasticity in adult animals is blocked by ZD7288.

(A) Voltages used in each portion of the plasticity experiment. Before CPA measures were made at –65 mV. Neurons without ZD7288 were returned to their resting membrane potential (RMP) and maintained there for the subsequent 40—60 minute recording period. Neurons with ZD7288 were held at –63 mV. All neurons were again held at –65 mV at the end of the experiment to collect after CPA measurements. (B) The time course of change in normalized R_{in} for VHC neurons with and without ZD7288. (C) Representative before and after CPA traces for measurement of R_{in} (performed at –65 mV). (D) Before and after CPA measurements of R_{in} and f_R (at –65 mV). Horizontal bars indicate average values and stars indicate a significant change with a paired statistical test ($p < 0.05$). (E) Average absolute percent change after CPA (for measures made at –65 mV). Error bars are standard error of the mean (S.E.M.).

V. Store depletion *h* plasticity is observed in the dendrites of adult, not adolescent animals.

Although Narayanan et al. (2010) showed that plasticity in adolescent animals was expressed peri-somatically in neurons from the middle hippocampus, it was not known whether plasticity was peri-somatic in DHC and VHC neurons from adolescents. Dendrites of neurons from adolescent DHC and VHC were patched at distances 150–250 μm from the soma (DHC: 174.29 ± 13.56 μm; VHC: 155 ± 2.89 μm) and experiments were performed with the standard plasticity protocol. No changes were observed in R_{in} (Fig. 26A,B; DHC before CPA: 40.95 ± 3.54 MΩ; DHC after CPA: 41.66 ± 4.57 MΩ; $p > 0.05$; VHC before CPA: 52.98 ± 9.31 MΩ; VHC after CPA: 58.84 ± 11.51 MΩ; $p > 0.05$) or f_R (Fig. 26C; DHC before CPA: 5.14 ± 0.52 Hz; DHC after CPA: 5.20 ± 0.62 Hz; $p > 0.05$; VHC before CPA: 4.28 ± 0.59 Hz; VHC after CPA: 3.93 ± 0.69 Hz; $p > 0.05$) of dendrites in adolescent DHC or VHC neurons. The percentage decrease in R_{in} (Fig. 26B) and increase in f_R (Fig. 26C) were plotted as functions of recording distance from the soma (including the somatic data from Fig. 21,22), revealing that plasticity in DHC and VHC neurons from adolescents showed a dramatic decrease with distance from the soma. These results together with those from Narayanan et al, (2010) indicate that SD plasticity is peri-somatic in expression for CA1 pyramidal neurons across the dorso-ventral axis of the hippocampus in adolescent animals.

The results observed at somata of adult animals, however, have suggested differences in the nature of SD *h* plasticity between adolescent and adult animals. Previous descriptions of *h* channel plasticity in neurons have demonstrated that the sub-cellular distribution of *h* plasticity can vary greatly (Wang et al., 2003; Narayanan and Johnston, 2007; Campanac et al., 2008; Narayanan and Johnston, 2008; Narayanan et al., 2010b), providing reason to investigate whether there might be a different locus to plasticity in adult animals. Dendritic recordings were made from DHC and VHC neurons at distances 150–250 μm (DHC 178.75 ± 24.53 μm; VHC 185.83 ± 22.00 μm). Input resistance (R_{in}) was reduced after CPA in adult DHC and VHC neurons (Fig. 27A,B; DHC before CPA: 31.46 ± 4.61 MΩ; DHC after CPA: 24.03 ± 3.39 MΩ; $p < 0.05$; VHC before CPA: 47.95 ± 4.27 MΩ; VHC after CPA: 34.85 ± 5.08 MΩ; $p < 0.05$) and f_R increased for VHC, but not DHC neurons (Fig. 27C; DHC before CPA: 5.02 ± 0.49 Hz; DHC after CPA: 5.26 ± 0.13 Hz; $p > 0.05$; VHC before CPA: 4.00 ± 0.24 Hz; VHC after CPA: 4.61 ± 0.33 Hz; $p < 0.05$), indicating that SD plasticity is somato-dendritic in adult VHC neurons and dendritic in adult DHC neurons.

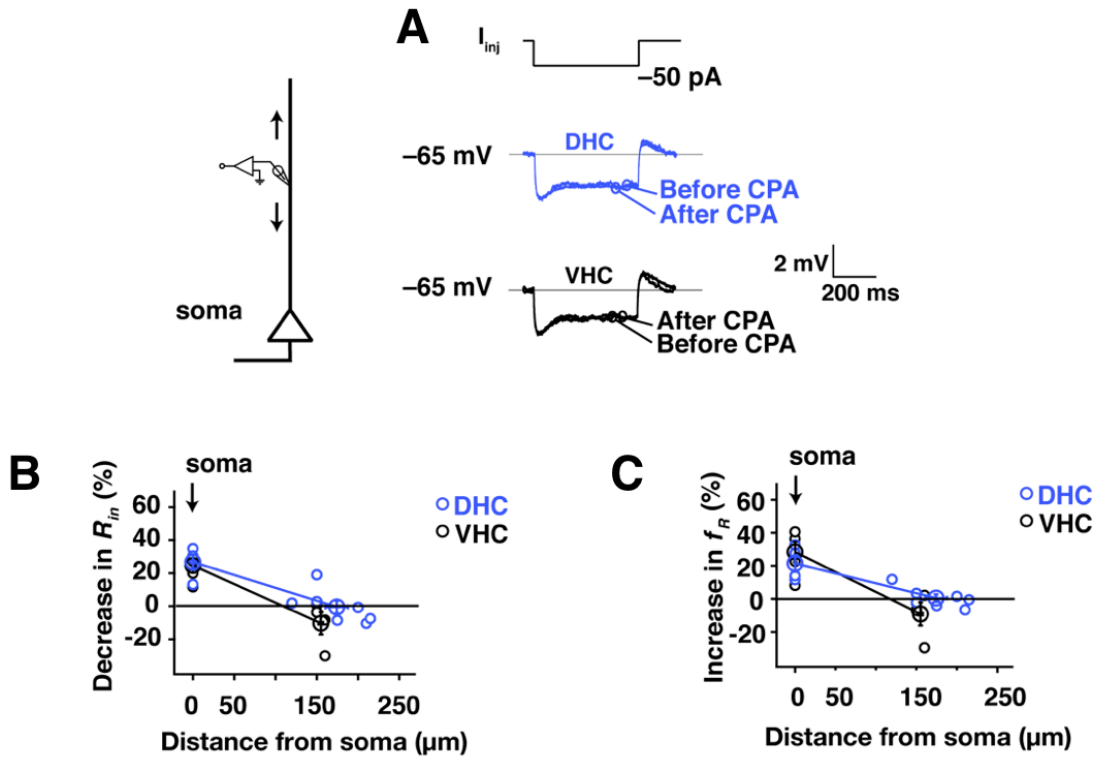

Figure 26: SD *h* plasticity is not observed in the dendrites of adolescent animals.

Whole-cell current clamp recordings were obtained from dendrites of DHC and VHC neurons. (A) Representative traces from measurements of R_{in} before and after CPA for DHC and VHC dendrites. All measurements made at –65 mV and current injection is –50 pA. (B) Percentage decrease in R_{in} versus distance from soma (µm) for adolescent animals. Somatic values included here to display the somato-dendritic relationship. (C) Percentage increase in f_R versus distance from soma (µm) for adolescent animals. Somatic values included here to display the somato-dendritic relationship.

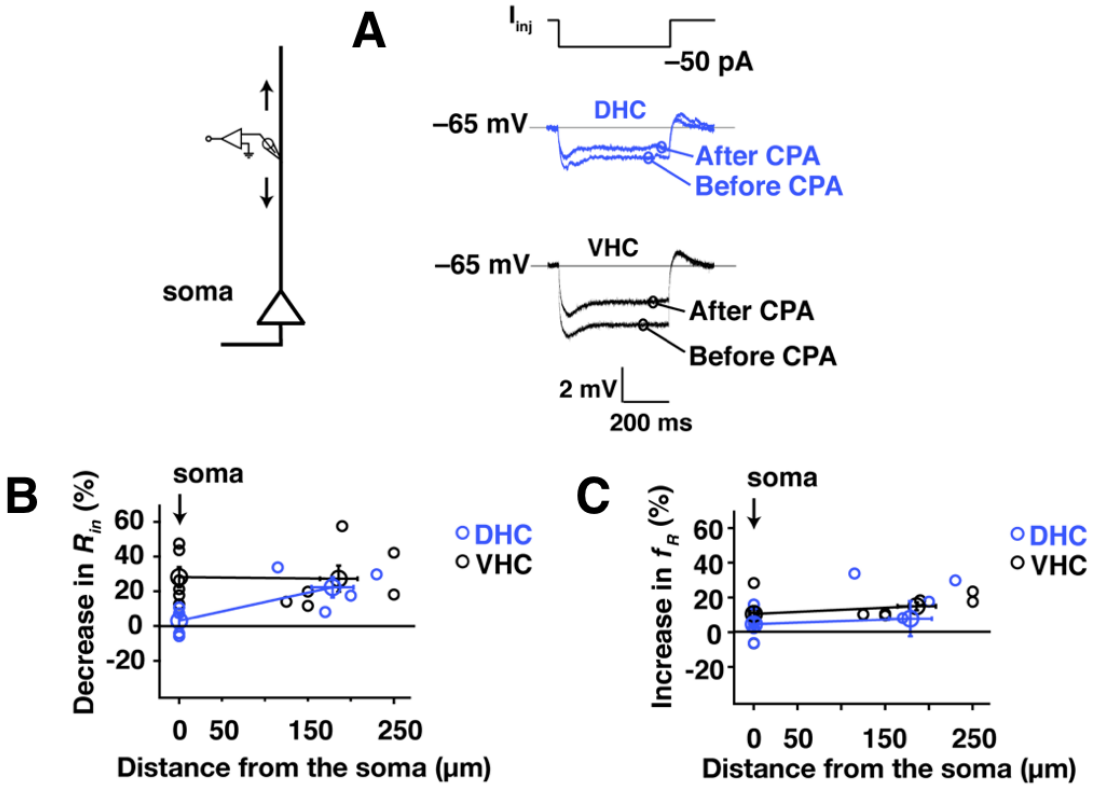

Figure 27: SD *h* plasticity is observed in the dendrites of adult animals.

Whole-cell current clamp recordings were obtained from dendrites of DHC and VHC neurons. (A) Representative traces from measurements of R_{in} before and after CPA for DHC and VHC dendrites from adult animals. All measurements were made at –65 mV and current injection is –50 pA. (B) Percentage decrease in R_{in} versus distance from soma (μm) for adult animals. Somatic values included here to display the somato-dendritic relationship. (C) Percentage increase in f_R versus distance from soma (μm) for adolescents. Somatic values included here to display the somato-dendritic relationship.

VI. Induction of store depletion *h* plasticity in adult animals is dependent on membrane voltage.

The relationship between the magnitude of plasticity expression and several basic intrinsic properties was examined to further understand the unique pattern of SD plasticity expression in adult animals. The most striking relationship was found when examining the percent change in R_{in} versus the initial RMP (Fig. 28). The case in which the smallest change in R_{in} was seen also had the most hyperpolarized RMP, which could explain why no plasticity was seen at the adult DHC soma. This raised the question of whether the expression of plasticity was dependent on the initial RMP (which is the voltage at which the cell was maintained during plasticity induction).

To test whether the membrane voltage during plasticity induction influenced the expression of plasticity, the experimental protocol was modified so that adult DHC neurons were maintained at more a more depolarized potential (–63 mV) during plasticity induction and adult VHC neurons were maintained at a more hyperpolarized potential (–66 mV; Fig. 29A). Rather surprisingly, these small deviations from the initial RMP were able to reverse plasticity expression for adult DHC and VHC neurons. The effectiveness of depolarization for producing plasticity on DHC neurons was seen when normalized R_{in} was monitored over time (Fig. 29B) and when R_{in} (Fig. 29C; before CPA: 75.80 ± 1.35 MΩ; after CPA: 54.30 ± 8.13 MΩ) and f_R (Fig. 29D; before CPA: 3.07 ± 0.30 Hz;

after CPA: 3.58 ± 0.42 Hz) were measured at –65 mV before and after CPA. Hyperpolarization of VHC neurons blocked the reduction in percent R_{in} (Fig. 29B) over time and the changes in R_{in} (Fig. 29C; before CPA: 88.71 ± 20.03 MΩ; after CPA: 84.80 ± 19.58 MΩ; reduction of R_{in}: 3.91 ± 1.52 MΩ) and f_R (Fig. 29D; before CPA: 3.96 ± 0.34 Hz; after CPA: 3.93 ± 0.19 Hz; increase in f_R: –0.03 ± 0.17 Hz) before and after CPA. These results, when put in the context of what was seen when induction was performed at each cell's initial RMP (Fig. 30), suggested that a voltage-dependent change in the range of a few millivolts is capable of determining whether SD plasticity occurs in adult DHC and VHC neurons.

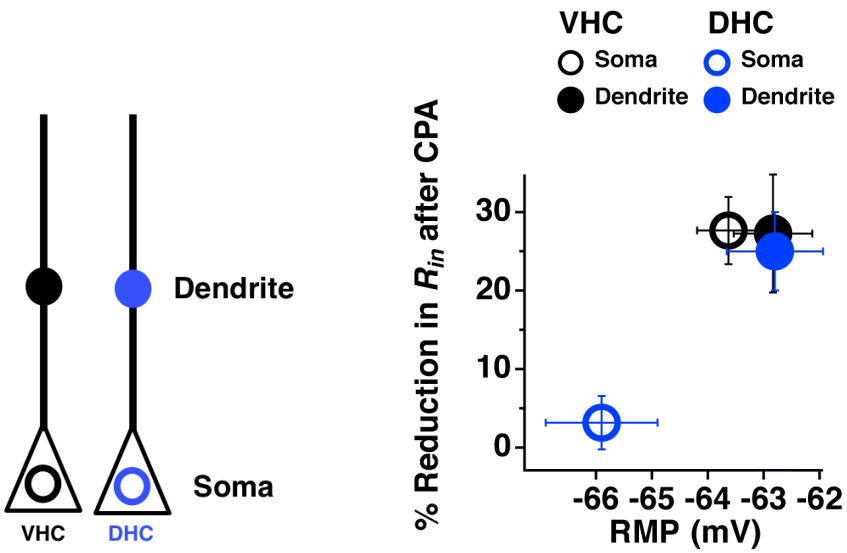

Figure 28: Percent reduction in input resistance after SD *h* plasticity versus resting membrane potential

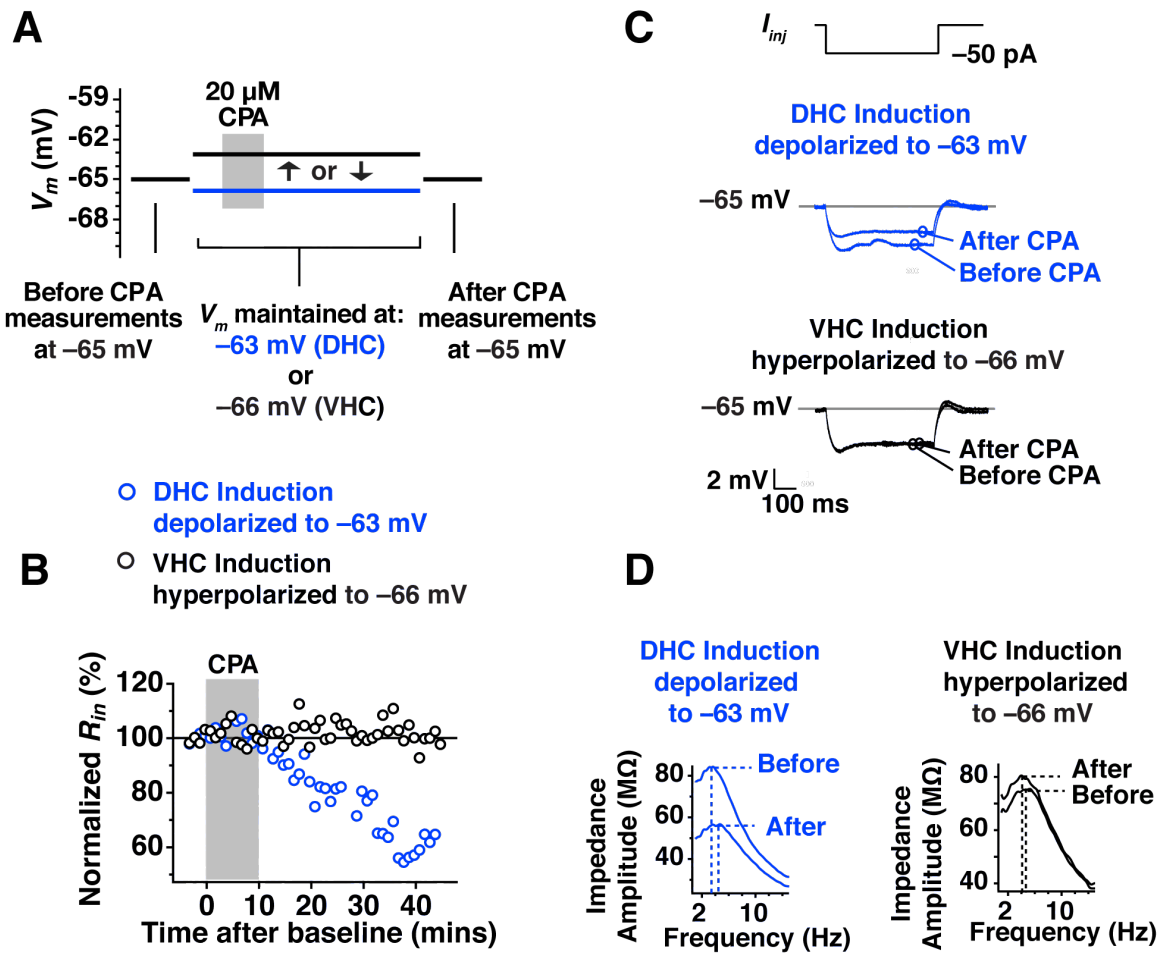

Figure 29: Induction of SD *h* plasticity is dependent on membrane voltage.

(A) Voltages used in each portion of the plasticity experiment. Before CPA measurements (R_{in} and f_R) were made at –65 mV. Instead of maintaining neurons at their initial RMP, DHC neurons were maintained at the average initial RMP for a VHC neuron (–63 mV). Neurons were again held at –65 mV at the end of the experiment to collect after CPA measurements. (B) Change in normalized R_{in} (%) over time. (C) Representative traces from measurements of R_{in} before and after CPA for DHC neurons depolarized to –63 mV during induction and VHC neurons hyperpolarized to –66 mV during induction. Before and after measurements were made at –65 mV and current injection is –50 pA. (D) Example impedance profiles from measurement of f_R before and after CPA for DHC neurons depolarized to –63 mV during induction and VHC neurons hyperpolarized to –66 mV during induction. Before and after measurements of f_R were made at –65 mV.

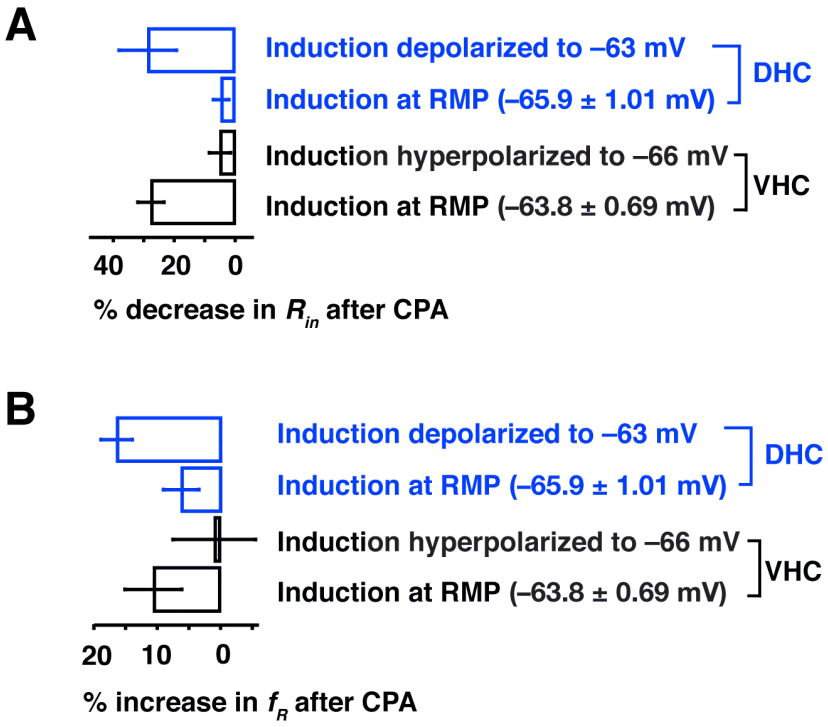

Figure 30: Summary of the effects of membrane voltage on SD *h* plasticity

Summary of results before and after CPA for % change in R_{in} (A) and f_R (B).

VII. Voltage-dependence of store depletion *h* plasticity in adult animals involves activation of *L*-type channels

L-type channels can be activated in the examined voltage range for plasticity induction in CA1 pyramidal neurons of the hippocampus (Magee et al., 1996). To test the hypothesis that *L*-type channels may contribute to SD *h* plasticity in adult, but not adolescent animals, experiments were performed in the presence of the *L*-type channel blocker nimodipine (10 μM). Nimodipine did not significantly change the initial RMP (adolescent VHC with nimodipine: –62.67 ± 1.45 mV; adult VHC with nimodipine –63.50 ± 0.65 mV) so induction was performed at each cell's initial RMP as before (Fig. 31A). Consistent with the signaling mechanisms underlying SD *h* plasticity in the middle hippocampus of adolescent animals (Narayanan et al., 2010b), nimodipine did not influence the expression of SD *h* plasticity in VHC neurons from adolescents (Appendix, Table 3), but did block plasticity in adult VHC neurons (Fig. 31B). Measurement of R_{in} at –65 mV before and after CPA showed that R_{in} was not significantly reduced by store depletion in the presence of nimodipine (Fig. 31C; Appendix, Table 3; before CPA: 65.35 ± 2.42 MΩ; after CPA: 57.70 ± 7.62 MΩ; $p > 0.05$). f_R also showed no change after CPA (Fig. 31D; Appendix, Table 3; before CPA: 4.11 ± 0.42 Hz; after CPA: 4.27 ± 0.31 Hz; $p > 0.05$).

Experiments were also performed to test whether the maintained depolarization applied to adult DHC neurons (in Fig. 29) was capable of restoring

plasticity in the presence of nimodipine. The percent change in R_{in} over time for a representative example is shown in Fig. 32B. No significant change in R_{in} was seen when adult DHC neurons were depolarized in the presence of nimodipine (Fig. 32C; Appendix, Table 3; before CPA: 64.43 ± 4.46 MΩ; after CPA: 59.12 ± 0.56 MΩ; $p > 0.05$), nor was a change seen for f_R (Fig. 32; Appendix, Table 3; before CPA: 3.06 ± 0.29 Hz; after CPA: 3.43 ± 0.32 Hz; $p > 0.05$). Thus, the voltage-dependence of SD *h* plasticity induction in adult animals appears to involve activation of *L*-type channels in DHC and VHC neurons.

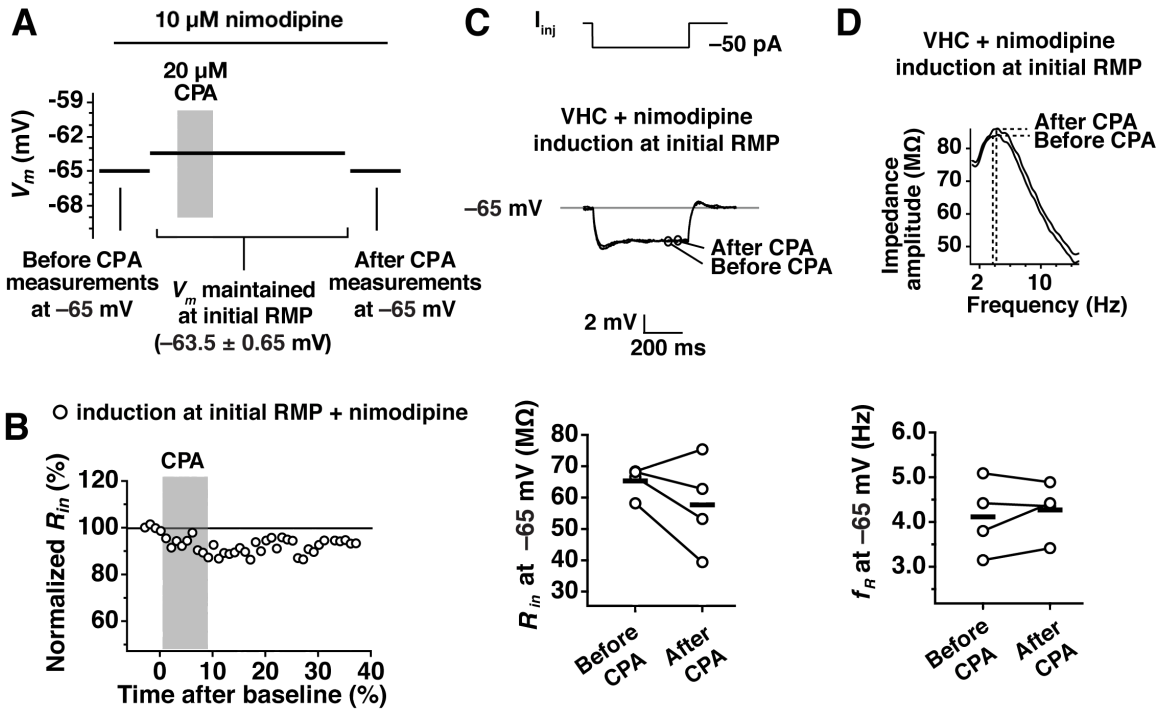

Figure 31: SD *h* plasticity in adult ventral neurons involves activation of L-type channels.

(A) Voltages used in each portion of the plasticity experiment. Before CPA measurements (R_{in} and f_R) were made at –65 mV. Neurons were then returned to their resting membrane potential (RMP) and maintained there for the subsequent 40—60 minute recording period. Neurons were again held at –65 mV at the end of the experiment to collect after CPA measurements. All measurements are made in the presence of 10 μM nimodipine. (B) Change in normalized R_{in} over time. (C) Representative traces for measurement of R_{in} before and after CPA in the presence of nimodipine for VHC neurons (above). Values for all examined cells (below). Horizontal lines are averages. (D) Representative impedance profiles before and after CPA in the presence of nimodipine for adult VHC neurons (above). Values of f_R before and after CPA in the presence of nimodipine (below). Horizontal lines are average values.

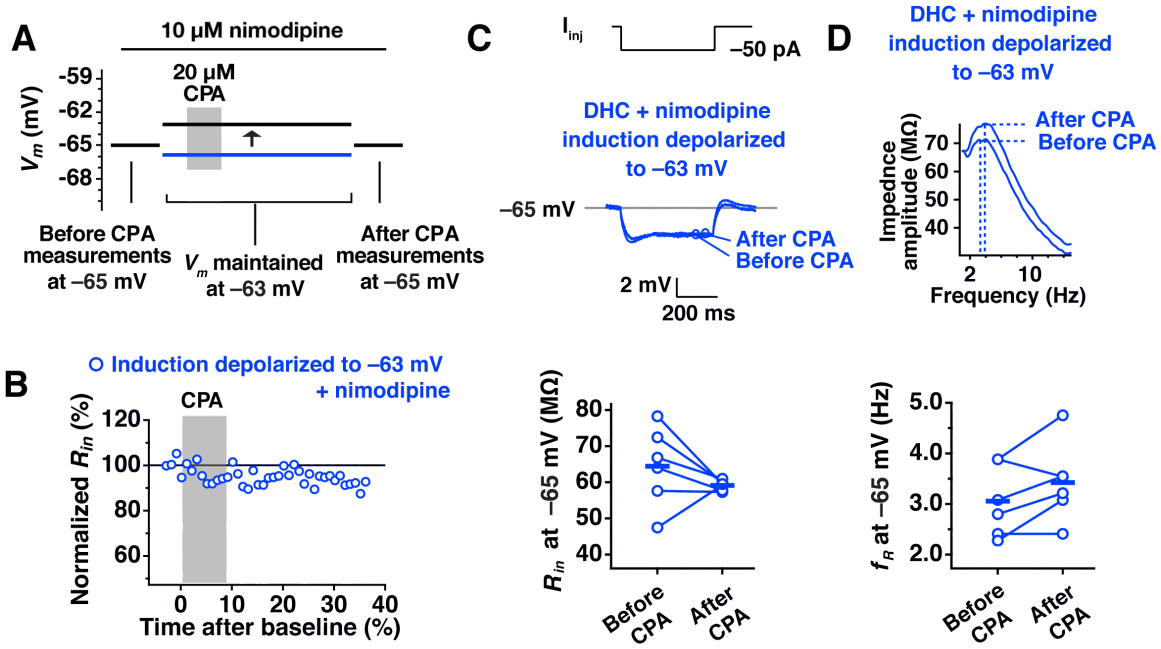

Figure 32: SD *h* plasticity in adult dorsal neurons involves activation of *L*-type channels.

(A) DHC neurons were maintained at –63 mV (similar to experiments in Fig 30,31), though this time in the presence of 10 μM nimodipine. (B) Change in normalized R_{in} over time. (C) Representative traces for measurement of R_{in} before and after CPA in the presence of nimodipine for DHC neurons from mature adults (above). Values for all examined cells (below). Horizontal lines are averages. (D) Representative impedance profiles before and after CPA in the presence of nimodipine for adult VHC neurons (above). Values for f_R before and after CPA in the presence of nimodipine (below). Horizontal lines are average values.

Chapter 4: Discussion

I. Summary

This dissertation examined store depletion plasticity of *h* channels in DHC and VHC neurons from adolescent and adult animals. The following changes were found between these 2 ages: (1) loss of plasticity at the somata of DHC neurons with age; (2) a spatial shift in the locus of plasticity from adolescence to adulthood, where adolescents show a peri-somatic expression of plasticity and adults show somato-dendritic plasticity in VHC and dendritic plasticity in DHC neurons; (3) plasticity in adult animals is dependent on membrane voltage; and (4) The voltage-dependence of plasticity is at least partially mediated by the activation of *L*-type voltage gated Ca^{2+} channels (Summarized in Fig. 33).

II. Age-dependent shift in the somato-dendritic location of store depletion *h* plasticity

A. Adolescent animals

Although DHC and VHC neurons in adolescent animals have distinct baseline intrinsic properties (RMP, R_{in}, f_R), the percent changes in R_{in} and f_R following SD

h plasticity were comparable. The percent reduction in R_{in}, and the percent increase in f_R were very similar across dorsal, ventral and middle hippocampal neurons (Fig. 26; Narayanan et al., 2010). Neuronal models, however, suggest a non-linear relationship between f_R and HCN channel density, implying that the number of *h* channels required to produce a change in f_R from 3.39 to 4.11 Hz (observed for adolescent DHC neurons) are different than the number of channels required to produce a change from 4.51 to 5.80 Hz (observed for adolescent VHC neurons) (Hutcheon et al., 1996; Narayanan and Johnston, 2007).

B. Adult animals

With age, significant changes in SD *h* plasticity were observed. Although there was no plasticity at the soma of adult DHC neurons, a reduction in R_{in} of adult DHC dendrites after SD *h* plasticity was seen. In adult VHC neurons, a comparable reduction in R_{in} to what was observed in adolescent VHC neurons occurred, however the increase in f_R was not as large (Figure 24). Frequency-dependent signals show greater distance-dependent attenuation compared with steady-state signals (Rall and Segev, 1985; Spruston et al., 1993), suggesting that the location of plasticity in adult animals may have shifted to the dendrites with age. It's possible that a dendritic change in *h* channels measured at the soma could detect a change in R_{in} without a comparable change in f_R due to

these features of attenuation or the differential influence of dendritic *h* channels on somatic R_{in} and f_R (Rathour and Narayanan, 2012).

C. Possible mechanisms for the spatial spread of SD *h* plasticity

The observed spatial extent of SD *h* plasticity varied based on age and hippocampal region even though the store depletion agent, CPA, was delivered by bath application and the distribution of SERCA is thought to be uniform in hippocampal neurons (Jacob et al., 2005). Assuming that there are no dorso-ventral differences or adolescent to adult changes in SERCA distribution, it is possible that another Ca^{2+} signaling component mediates the spatial extent of plasticity.

It was suggested that the peri-somatic SD *h* plasticity observed by Narayanan et al. (2010) could be due to the InsP3R-interacting molecule chromogranin B (CGB) (Schmidt and Ehrlich, 2010), which increases the open probability of the InsP3R and is expressed in the soma and proximal dendrites of hippocampal neurons (Jacob et al., 2005). If CGB becomes more highly expressed in dendrites with age, this could explain why SD *h* plasticity is seen only in the dendrites of adult animals. Additionally, one study showed that between 2 and 10 weeks of age, InsP3R1 expression shifts from a high density in the proximal apical dendrites to a uniform dendritic distribution in CA1 pyramidal neurons (Hertle and Yeckel, 2007). Thus, an age-dependent shift in

the InsP3R or its associated molecules could be responsible for the observed results. Other candidates of the neuronal Ca^{2+} signaling toolkit such as calcium activated PKA, SOC and *L*-type channels could also lend to the observed spatial shift in plasticity.

D. Implications for synaptic integration

A peri-somatic increase in *h*, as was observed for adolescent animals, should have a different impact on synaptic integration than the dendritic and somato-dendritic increase in *h* observed for adult neurons. Because action potential initiation occurs near the soma, the observed peri-somatic reduction in R_{in} should have an impact on the integration of all dendrite-to-soma spreading events, regardless of where they originate. The dendritic changes in R_{in} that were observed for adult animals, however, could be capable of preferentially influencing some inputs and not others. For example, if over-excitation is occurring at a select subset of synapses, it might be advantageous for the neuron to reduce excitability in the dendritic region where the over-excitation is occurring and not for the entire cell. Sub-cellular localization of intrinsic plasticity has a proposed role in mnemonic memory processes, where the throughput of specific synapses may be affected (Zhang and Linden, 2003). Our results demonstrate that the sub-cellular extent of intrinsic plasticity is highly age and region-

dependent; it would be interesting to see if similar trends exist with associative forms of intrinsic plasticity such as theta-burst pairing plasticity.

III. Store depletion *h* plasticity induction depends on membrane voltage and activation of *L*-type channels in adult neurons.

Somatic measurements of SD *h* plasticity revealed that plasticity occurred in somata of adolescent, but not adult DHC neurons. Plasticity measured at somata of adult DHC neurons could be induced by manipulation of membrane voltage in the depolarizing direction, which appears to be at least partially dependent on activation of *L*-type channels. Manipulation of membrane voltage in the opposite (hyperpolarizing) direction is capable of blocking plasticity for adult VHC neurons. An *L*-type channel component of the SD *h* plasticity mechanism, thus, appears to emerge between adolescence and adulthood. Although comparisons of *L*-type channel expression between adolescence and adulthood are lacking, age-dependent increases in *L*-type channel activity have been described with age for middle-aged rats and older (Thibault and Landfield, 1996; Gant et al., 2006).

L-type channels have several established links with store-dependent processes. The frequency of store-dependent Ca^{2+} events or “puffs” in the dendrites of pyramidal neurons are changed with membrane voltage and *L*-type channel activation (Manita and Ross, 2009). The function of these events is not clear, though they undergo age-dependent changes in magnitude and kinetics

(Miyazaki et al., 2012). *L*-type channels were also recently linked with store-operated Ca^{2+} entry. *L*-type VGCC are suppressed by Orai1-STIM1 channel complexes through a structural relationship (Park et al., 2010; Wang et al., 2010), but the age-dependence of this phenomenon has not been investigated. Future experiments could explore if this suppression is specific to adolescents, thereby leading to a role for *L*-type VGCC in adult SD *h* plasticity, but not in adolescents.

IV. Implications for disease vulnerability

The unfolded protein response (UPR) is an extensively studied response initiated with ER stress. The UPR activates transcription of genes that enhance protein folding, inhibit translation and promote degradation of misfolded proteins. The UPR is adaptive, but if ER stress is prolonged, the UPR signaling pathway will revert to apoptosis and trigger cell death (Verkhratsky, 2005). The adaptive components of the UPR signaling pathway are reduced with age (Kesslak et al., 1995; Hussain and Ramaiah, 2007; Naidoo et al., 2008; Gavilán et al., 2009; Novati et al., 2011); it is suggested that age-dependent modification of the UPR is responsible for susceptibilities to disease and cellular death (Saxena and Caroni, 2011; Brown and Naidoo, 2012; Schipanski et al., 2013). If SD *h* plasticity is an alternate form of adaptation to ER stress, as has been proposed (Narayanan et al., 2010b), the findings of the present study could provide a basis

for differences in ER stress related vulnerabilities that occur between adolescence and adulthood.

Specifically, the finding that SD *h* plasticity is not expressed in the dendrites of adolescent animals, though it is in adult animals, could provide a mechanism for increased vulnerability in adolescent animals. The highest density of excitatory synapses arrives at the dendrites of CA1 pyramidal neurons (Megías et al., 2001), thus suggesting that reductions of excitability in the dendrites may have the greatest impact on the neuron's ability to adapt to incoming stressors (Fig. 34). Depolarization of neuronal membrane voltage may initiate rises in cytoplasmic Ca^{2+} through voltage gated Ca^{2+} channels. A reduction in input resistance, as was observed in the dendrites of adult animals should, thus, reduce the likelihood that cytoplasmic rises in Ca^{2+} occur in response to depolarizing synaptic inputs. In the case of adolescent animals, no such reduction of input resistance occurred after store depletion. This indicates that depolarizing synaptic inputs in adolescents would continue to cause cytoplasmic rises in Ca^{2+}, which could further stress the cell and potentially lead cell death and pathology.

In the introduction of this dissertation, several parallels were discussed between adolescent disease vulnerabilities and disruptions of intracellular Ca^{2+} and endoplasmic reticulum function. The adolescent brain is more susceptible to epilepsy (Kesslak et al., 1995), sleep loss (Novati et al., 2011), alcohol exposure (Markwiese et al., 1998), behavioral stress (Cao et al., 2013), and traumatic

injury (McKee et al., 2009; Greco et al., 2013). Interestingly, all of these stressors are also associated with disruptions of ER function and/or disruptions of intracellular Ca^{2+}. Sleep loss and alcohol exposure both cause increases in markers of ER stress (Naidoo et al., 2008; Kitamura, 2013); epilepsy causes changes in intracellular Ca^{2+} release and sequestration (Pal et al., 2001); social isolation, a form of behavioral stress, results in changes in the expression of calcium binding proteins (Harte et al., 2007; Pascual et al., 2007) and traumatic brain injury causes release and depletion of Ca^{2+} from internal stores (Gemes et al., 2009; Weber, 2012). The work included in this dissertation provides evidence that the ability of CA1 neurons in the hippocampus to adapt to disruptions of the ER Ca^{2+} stores is lesser in adolescents when compared with adults. Further investigation of pathological states in adolescent animals could establish whether the stressors discussed above are connected to disruptions of intracellular Ca^{2+}.

V. Connection to the behaving animal

The experiments that comprise this dissertation work were all performed in brain slices in the constant presence of synaptic blockers. Neurons in the behaving animal, however, are highly influenced by incoming synaptic inputs. Additionally, a majority of the experiments performed in this dissertation were performed at a constant membrane potential while we know that neurons in the behaving animal rarely sit at a constant membrane potential. Due to the fact that this work is

primarily concerned with voltage-gated conductances, however, the precise control of membrane voltage in these experiments was a requirement. Despite this fact, it remains difficult to directly relate what has been observed here to what would happen while the animal is behaving.

The relative amounts of depolarizing, excitatory and hyperpolarizing, inhibitory input experienced by a CA1 neuron in a behaving animal are expected to vary based on the behavioral state. Although the “up” and “down” states created by such inputs create an unstable membrane voltage, the membrane voltage at which these inputs are superimposed on could still be capable of influencing the induction of a form of plasticity such as store depletion plasticity. Furthermore, the finding that the induction of store depletion plasticity in adult animals is dependent on a difference of membrane voltage of only a few millivolts could mean that the induction of SD plasticity is highly dependent on the relative amounts of inhibitory and excitatory input, which depend on the current behavioral state of the animal. With advancement of *in vivo* intracellular recording techniques, these and other topics could be addressed.

VI. Final thoughts about age

A large number of studies that examine the disruptions of internal Ca^{2+} with age choose only two disparate time points, which are usually include a young adult, or adolescent time point and one aged time point, which for rats is close to 2

years old (Fig. 35). The findings of the present dissertation, however, show that significant changes in cellular physiology occur between adolescence and adulthood. With this in mind, studies regarding age-dependent physiological changes in neurons may benefit from a selection of a range of time points rather than only two.

VII. Conclusions

This dissertation work demonstrates that plasticity of *h* channels in response to depletion of calcium stores from the ER is significantly different between adolescence and adulthood and that these differences are highly dependent on the dorso-ventral location in the hippocampus. A shift in plasticity location from a peri-somatic expression in adolescent DHC and VHC neurons to a dendritic and somato-dendritic expression of plasticity for adult DHC and VHC neurons was observed. This age-dependent shift in plasticity location could function to specifically alter the throughput of synapses that may be causing over-excitation and cellular stress. Furthermore, an age-dependent introduction of *L*-type channels to the plasticity mechanism that appeared to underlie the differences in plasticity observed at the soma of adult DHC and VHC neurons was observed. The present observations may be relevant for age and region-dependent disease vulnerabilities in the mammalian brain.

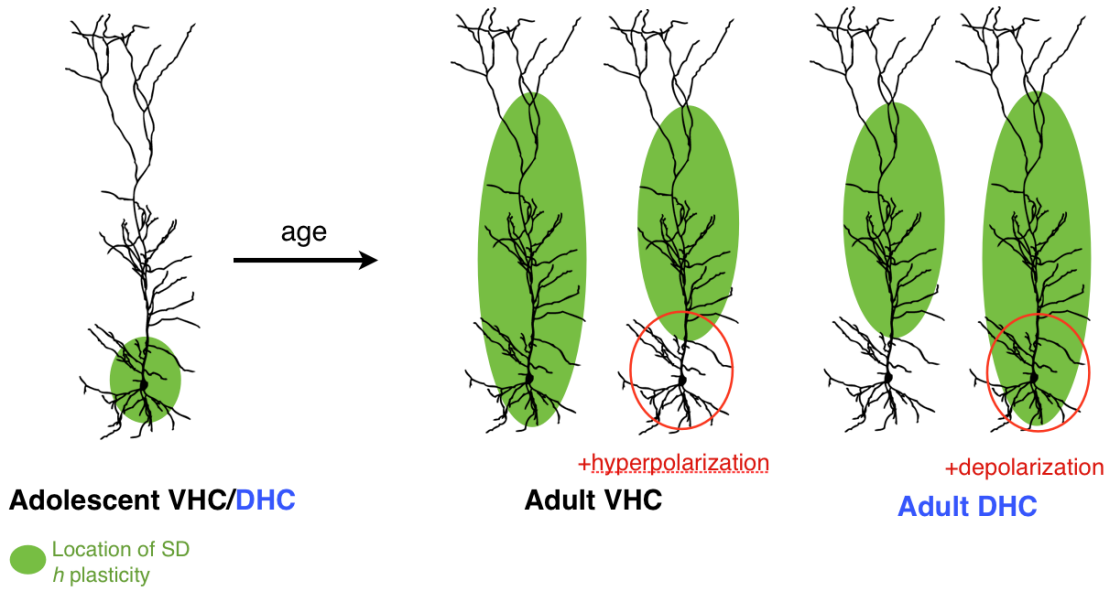

Figure 33: Age- and location-dependent changes in SD *h* plasticity

Between adolescence and adulthood: a loss of plasticity occurred at the somata of DHC neurons; a spatial shift in the locus of plasticity occurred; a voltage-dependent mechanism of plasticity induction that is at least partially mediated by the activation of *L*-type voltage gated Ca^{2+} channels was observed in adults and not adolescents.

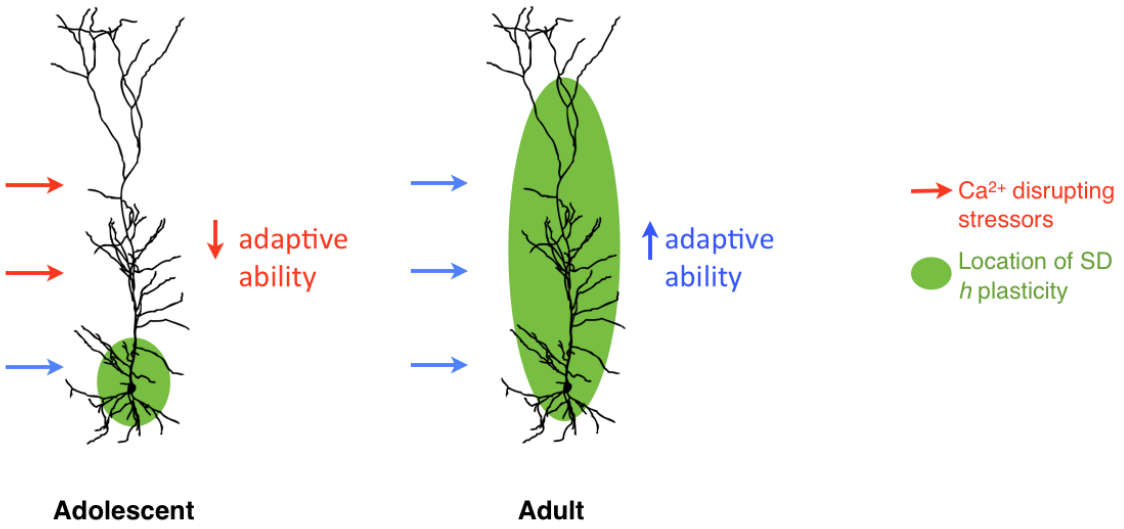

Figure 34: The dendrites of adolescent animals may be more vulnerable to Ca^{2+} disrupting cellular stressors.

In adults, but not adolescents, store depletion *h* plasticity was observed in the dendrites, which is the site at which the highest density of synaptic inputs arrives. Depolarizing inputs which produce rises in intracellular Ca^{2+} do not have a mechanism to reduce excitability and lower the likelihood of cytoplasmic rises in Ca^{2+} for adolescent animals, which could indicate a source of increased vulnerability in adolescent animals.

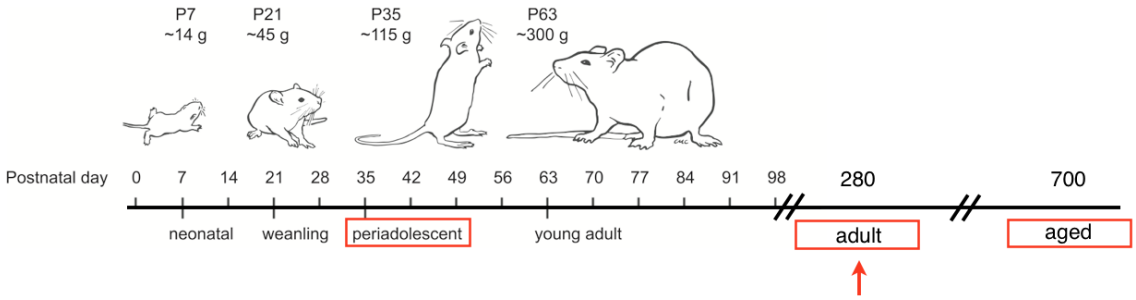

Figure 35: Consideration of age groups in the study of age-dependent intracellular Ca^{2+} disruptions.

A large number of studies that examine the disruptions of intracellular Ca^{2+} choose two disparate time points. The work of this dissertation shows that cell physiological changes may be significant between adolescence and adulthood. Figure modified from (McCutcheon and Marinelli, 2009).

Appendix

Table 1. Measurements sensitive to *h* channels and their values before and after CPA for adolescent DHC and VHC neurons

Measurement (units)	Before CPA	After CPA	Significance
Adolescent DHC (n = 4)			
RMP (mV)	–64.50 ± 0.87	–59.88 ± 1.23	$p < 0.05$
R_{in} (MΩ)	66.21 ± 7.39	49.52 ± 9.03	$p < 0.05$
f_R (Hz)	3.39 ± 0.14	4.11 ± 0.15	$p < 0.05$
Adolescent VHC (n = 4)			
RMP (mV)	–62.88 ± 1.01	–59.50 ± 0.87	$p < 0.05$
R_{in} (MΩ)	89.04 ± 7.35	66.62 ± 5.01	$p < 0.05$
f_R (Hz)	4.51 ± 0.26	5.80 ± 0.49	$p < 0.05$
All values are means ± standard error of the mean (S.E.M.)			

Table 1: Measurements sensitive to h channels and their values before and after CPA for adolescent DHC and VHC neurons. Resting membrane potential (RMP), input resistance (R_{in}) and resonance frequency (f_R) before and after CPA for DHC (top) and VHC (bottom) neurons from adolescent animals. R_{in} and f_R were measured at –65 mV; all values are means ± standard error of the mean (S.E.M.).

Table 2. Measurements sensitive to *h* channels and their values before and after CPA for adult DHC and VHC neurons

Measurement (units)	Before CPA	After CPA	Significance
Adult DHC (n = 6)			
RMP (mV)	–65.90 ± 1.01	–65.80 ± 1.07	ns
R_{in} (MΩ)	59.59 ± 2.52	57.76 ± 2.82	ns
f_R (Hz)	3.49 ± 0.14	3.66 ± 0.24	ns
Adult VHC (n = 5)			
RMP (mV)	–63.83 ± 0.69	–61.50 ± 1.65	ns
R_{in} (MΩ)	81.94 ± 3.46	58.00 ± 3.25	$p < 0.05$
f_R (Hz)	3.95 ± 0.17	4.40 ± 0.36	$p < 0.05$
Adult VHC +ZD7288 (n = 5)			
RMP (mV)	–68.20 ± 1.24	–70.00 ± 1.92	ns
R_{in} (MΩ)	97.09 ± 7.02	102.96 ± 7.98	ns
f_R (Hz)	1.12 ± 0.12	1.00 ± 0.00	ns
All values are means ± standard error of the mean (S.E.M.)			

Table 2: Measurements sensitive to h channels and their values before and after CPA for adult DHC and VHC neurons. Resting membrane potential (RMP), input resistance (R_{in}) and resonance frequency (f_R) before and after CPA for adult DHC

neurons (top), adult VHC neurons (middle) and adult VHC neurons in the presence of ZD7288 (bottom). R_{in} and f_R were measured at –65 mV; all values are means ± standard error of the mean (S.E.M.).

Table 3. Measurements sensitive to *h* channels and their values before and after CPA for DHC and VHC neurons in the presence of nimodipine

Measurement (units)	Before CPA	After CPA	Significance
Adolescent VHC + nimodipine (n = 4)			
RMP (mV)	–62.67 ± 1.45	–57.67 ± 2.33	$p < 0.05$
R_{in} (MΩ)	72.07 ± 2.98	54.50 ± 2.63	$p < 0.05$
f_R (Hz)	3.57 ± 0.233	4.60 ± 0.26	$p < 0.05$
Adult VHC + nimodipine (n = 4)			
RMP (mV)	–63.50 ± 0.64	–61.75 ± 0.48	ns
R_{in} (MΩ)	65.35 ± 2.42	57.70 ± 7.61	ns
f_R (Hz)	4.11 ± 0.42	4.27 ± 0.31	ns
Adult DHC + nimodipine + depolarization (n = 6)			
RMP (mV)	–65.17 ± 0.40	–63.33 ± 0.81	ns
R_{in} (MΩ)	64.43 ± 4.46	59.12 ± 0.56	ns
f_R (Hz)	3.06 ± 0.29	3.43 ± 0.32	ns
All values are means ± standard error of the mean (S.E.M.)			

Table 3: Measurements sensitive to h channels and their values before and after CPA for adult DHC and VHC neurons in the presence of nimodipine. Resting membrane potential (RMP), input resistance (R_{in}) and resonance frequency (f_R) before and after CPA for adolescent VHC (top), adult VHC (middle) and adult DHC neurons with depolarization during induction (bottom). All experiments were performed in the continuous presence of nimodipine (10 μM). R_{in} and f_R were measured at –65 mV; all values are means ± standard error of the mean (S.E.M.).

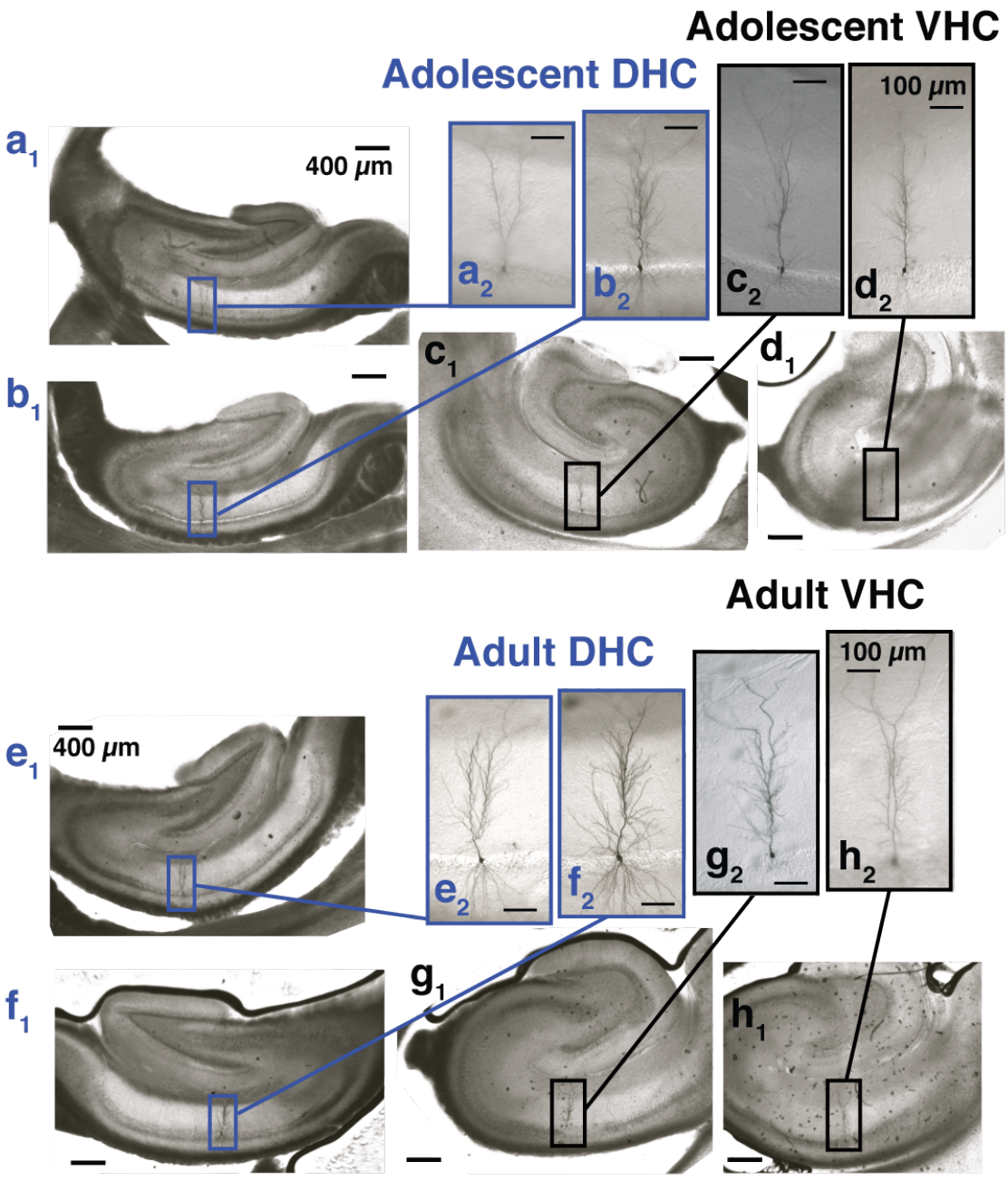
Adolescent VHC
Adolescent DHC
100 μm
400 μm
a1
a2
b2
c2
d2
b1
c1
d1
Adult VHC
Adult DHC
100 μm
400 μm
e1
e2
f2
g2
h2
f1
g1
h1

Figure S1: Examples of processed dorsal and ventral slices from adolescent and adult animals

(A,B) Example DHC slices from adolescent animals and processed, neurobiotin filled neurons. (C,D) Example VHC slices from adolescent animals and processed, neurobiotin filled neurons. (E,F) Example DHC slices from adult animals and processed, neurobiotin filled neurons. (G,H) Example VHC slices from adolescent animals and processed, neurobiotin filled neurons.

Bibliography

Alberts B (2008) Molecular Biology of the Cell. Garland Pub.

Bannerman DM, Rawlins JNP, McHugh SB, Deacon RMJ, Yee BK, Bast T, Zhang W-N, Pothuizen HHJ, Feldon J (2004) Regional dissociations within the hippocampus--memory and anxiety. Neurosci Biobehav Rev 28:273–283.

Berridge MJ (2002) The endoplasmic reticulum: a multifunctional signaling organelle. Cell Calcium 32:235–249.

Biel M, Wahl-Schott C, Michalakis S, Zong X (2009) Hyperpolarization-activated cation channels: from genes to function. Physiological Reviews 89:847–885.

Brown MK, Naidoo N (2012) The endoplasmic reticulum stress response in aging and age-related diseases. Front Physiol 3:263.

Cahalan MD (2009) STIMulating store-operated Ca(2+) entry. Nat Cell Biol 11:669–677.

Campanac E, Daoudal G, Ankri N, Debanne D (2008) Downregulation of Dendritic Ih in CA1 Pyramidal Neurons after LTP. Journal of Neuroscience 28:8635–8643.

Cao X, Huang S, Cao J, Chen T, Zhu P, Zhu R, Su P, Ruan D (2013) The timing of maternal separation affects morris water maze performance and long-term potentiation in male rats. Dev Psychobiol.

Ciccia A, Elledge SJ (2010) The DNA damage response: making it safe to play with knives. Mol Cell 40:179–204.

Cui-Wang T, Hanus C, Cui T, Helton T, Bourne J, Watson D, Harris KM, Ehlers MD (2012) Local zones of endoplasmic reticulum complexity confine cargo in neuronal dendrites. Cell 148:309–321.

Dougherty KA, Islam T, Johnston D (2012) Intrinsic Excitability of CA1 Pyramidal Neurones from the Rat Dorsal and Ventral Hippocampus. The Journal of Physiology.

Dougherty KA, Nicholson DA, Diaz L, Buss EW, Neuman KM, Chetkovich DM, Johnston D (2013) Differential expression of HCN subunits alters voltage-dependent gating of h-channels in CA1 pyramidal neurons from dorsal and ventral hippocampus. Journal of Neurophysiology 109:1940–1953.

Fanselow MS, Dong H-W (2010) Are the dorsal and ventral hippocampus functionally distinct structures? Neuron 65:7–19.

Fulda S, Gorman AM, Hori O, Samali A (2010) Cellular stress responses: cell survival and cell death. Int J Cell Biol 2010:214074.

Gant JC, Sama MM, Landfield PW, Thibault O (2006) Early and simultaneous emergence of multiple hippocampal biomarkers of aging is mediated by Ca2+-induced Ca2+ release. J Neurosci 26:3482–3490.

Gavilán MP, Pintado C, Gavilán E, Jiménez S, Ríos RM, Vitorica J, Castaño A, Ruano D (2009) Dysfunction of the unfolded protein response increases neurodegeneration in aged rat hippocampus following proteasome inhibition. Aging Cell 8:654–665.

Gemes G, Rigaud M, Weyker PD, Abram SE, Weihrauch D, Poroli M, Zoga V, Hogan QH (2009) Depletion of calcium stores in injured sensory neurons: anatomic and functional correlates. Anesthesiology 111:393–405.

Greco T, Hovda D, Prins M (2013) The Effects of Repeat Traumatic Brain Injury on the Pituitary in Adolescent Rats. J Neurotrauma.

Grigoryan G, Korkotian E, Segal M (2012) Selective facilitation of LTP in the ventral hippocampus by calcium stores. Hippocampus 22:1635–1644.

Harte MK, Powell SB, Swerdlow NR, Geyer MA, Reynolds GP (2007) Deficits in parvalbumin and calbindin immunoreactive cells in the hippocampus of isolation reared rats. J Neural Transm 114:893–898.

Hertle DN, Yeckel MF (2007) Distribution of inositol-1,4,5-trisphosphate receptor isotypes and ryanodine receptor isotypes during maturation of the rat hippocampus. NSC 150:625–638.

Hollien J (2013) Biochimica et Biophysica Acta. BBA - Molecular Cell Research:1–6.

Holmes GL (1997) Epilepsy in the developing brain: lessons from the laboratory and clinic. Epilepsia 38:12–30.

Hussain SG, Ramaiah KVA (2007) Reduced eIF2alpha phosphorylation and increased proapoptotic proteins in aging. Biochem Biophys Res Commun 355:365–370.

Hutcheon B, Miura RM, Puil E (1996) Models of subthreshold membrane resonance in neocortical neurons. Journal of Neurophysiology 76:698–714.

Jacob SN, Choe C-U, Uhlen P, DeGray B, Yeckel MF, Ehrlich BE (2005)

Signaling microdomains regulate inositol 1,4,5-trisphosphate-mediated intracellular calcium transients in cultured neurons. Journal of Neuroscience 25:2853–2864.

Kesslak JP, Yuan D, Neeper S, Cotman CW (1995) Vulnerability of the hippocampus to kainate excitotoxicity in the aged, mature and young adult rat. Neurosci Lett 188:117–120.

Kitamura M (2013) The unfolded protein response triggered by environmental factors. Semin Immunopathol 35:259–275.

Luik RM, Wang B, Prakriya M, Wu MM, Lewis RS (2008) Oligomerization of STIM1 couples ER calcium depletion to CRAC channel activation. Nature 454:538–542.

Magee JC (1998) Dendritic hyperpolarization-activated currents modify the integrative properties of hippocampal CA1 pyramidal neurons. J Neurosci 18:7613–7624.

Magee JC, Avery RB, Christie BR, Johnston D (1996) Dihydropyridine-sensitive, voltage-gated Ca2+ channels contribute to the resting intracellular Ca2+ concentration of hippocampal CA1 pyramidal neurons. Journal of Neurophysiology 76:3460–3470.

Manita S, Ross WN (2009) Synaptic activation and membrane potential changes modulate the frequency of spontaneous elementary Ca2+ release events in the dendrites of pyramidal neurons. Journal of Neuroscience 29:7833–7845.

Marcelin B, Lugo JN, Brewster AL, Liu Z, Lewis AS, McClelland S, Chetkovich DM, Baram TZ, Anderson AE, Becker A, Esclapez M, Bernard C (2012) Differential dorso-ventral distributions of Kv4.2 and HCN proteins confer distinct integrative properties to hippocampal CA1 pyramidal cell distal dendrites. Journal of Biological Chemistry 287:17656–17661.

Markwiese BJ, Acheson SK, Levin ED, Wilson WA, Swartzwelder HS (1998) Differential effects of ethanol on memory in adolescent and adult rats. Alcohol Clin Exp Res 22:416–421.

McCutcheon JE, Marinelli M (2009) Age matters. Eur J Neurosci 29:997–1014.

McKee AC, Cantu RC, Nowinski CJ, Hedley-Whyte ET, Gavett BE, Budson AE, Santini VE, Lee H-S, Kubilus CA, Stern RA (2009) Chronic traumatic encephalopathy in athletes: progressive tauopathy after repetitive head injury. J Neuropathol Exp Neurol 68:709–735.

Megías M, Emri Z, Freund TF, Gulyás AI (2001) Total number and distribution of

inhibitory and excitatory synapses on hippocampal CA1 pyramidal cells. NSC 102:527–540.

Miyazaki K, Manita S, Ross WN (2012) Developmental profile of localized spontaneous Ca(2+) release events in the dendrites of rat hippocampal pyramidal neurons. Cell Calcium. 422-432.

Moser MB, Moser EI, Forrest E, Andersen P, Morris RG (1995) Spatial learning with a minislab in the dorsal hippocampus. Proc Natl Acad Sci USA 92:9697–9701.

Naidoo N (2009) ER and aging-Protein folding and the ER stress response. Ageing Res Rev 8:150–159.

Naidoo N, Ferber M, Master M, Zhu Y, Pack AI (2008) Aging impairs the unfolded protein response to sleep deprivation and leads to proapoptotic signaling. Journal of Neuroscience 28:6539–6548.

Narayanan R, Dougherty KJ, Johnston D (2010a) Calcium store depletion induces persistent perisomatic increases in the functional density of h channels in hippocampal pyramidal neurons. Neuron 68:921–935.

Narayanan R, Dougherty KJ, Johnston D (2010b) Calcium Store Depletion Induces Persistent Perisomatic Increases in the Functional Density of h Channels in Hippocampal Pyramidal Neurons. Neuron 68:921–935.

Narayanan R, Johnston D (2007) Long-term potentiation in rat hippocampal neurons is accompanied by spatially widespread changes in intrinsic oscillatory dynamics and excitability. Neuron 56:1061–1075.

Narayanan R, Johnston D (2008) The h channel mediates location dependence and plasticity of intrinsic phase response in rat hippocampal neurons. Journal of Neuroscience 28:5846–5860.

Novati A, Hulshof HJ, Koolhaas JM, Lucassen PJ, Meerlo P (2011) Chronic sleep restriction causes a decrease in hippocampal volume in adolescent rats, which is not explained by changes in glucocorticoid levels or neurogenesis. Neuroscience 190:145–155.

Pal S, Sun D, Limbrick D, Rafiq A, DeLorenzo RJ (2001) Epileptogenesis induces long-term alterations in intracellular calcium release and sequestration mechanisms in the hippocampal neuronal culture model of epilepsy. Cell Calcium 30:285–296.

Palop JJ, Chin J, Mucke L (2006) A network dysfunction perspective on neurodegenerative diseases. Nature 443:768–773.

Parekh AB (2005) Store-Operated Calcium Channels. Physiological Reviews 85:757–810.

Park CY, Shcheglovitov A, Dolmetsch R (2010) The CRAC Channel Activator STIM1 Binds and Inhibits L-Type Voltage-Gated Calcium Channels. Science 330:101–105.

Pascual R, Zamora-León P, Catalán-Ahumada M, Valero-Cabré A (2007) Early social isolation decreases the expression of calbindin D-28k and dendritic branching in the medial prefrontal cortex of the rat. Int J Neurosci 117:465–476.

Rall W, Segev I (1985) Space-clamp problems when voltage clamping branched neurons with intracellular microelectrodes. In: Voltage and patch clamping with microelectrodes, pp 191–215. Springer.

Rathour RK, Narayanan R (2012) Influence Fields: A Quantitative Framework for the Representation and Analysis of Active Dendrites. Journal of Neurophysiology. 2313–2334.

Ron D, Walter P (2007) Signal integration in the endoplasmic reticulum unfolded protein response. Nat Rev Mol Cell Biol 8:519–529.

Saxena S, Caroni P (2011) Selective neuronal vulnerability in neurodegenerative diseases: from stressor thresholds to degeneration. Neuron 71:35–48.

Schipanski A, Lange S, Segref A, Gutschmidt A, Lomas DA, Miranda E, Schweizer M, Hoppe T, Glatzel M (2013) A novel interaction between aging and ER overload in a protein conformational dementia. Genetics 193:865–876.

Schmidt S, Ehrlich BE (2010) Unloading Intracellular Calcium Stores Reveals Regionally Specific Functions. Neuron 68:806–808.

Spacek J, Harris KM (1997) Three-dimensional organization of smooth endoplasmic reticulum in hippocampal CA1 dendrites and dendritic spines of the immature and mature rat. J Neurosci 17:190–203.

Spruston N, Jaffe DB, Williams SH, Johnston D (1993) Voltage- and space-clamp errors associated with the measurement of electrotonically remote synaptic events. Journal of Neurophysiology 70:781–802.

Terasaki M, Slater NT, Fein A, Schmidek A, Reese TS (1994) Continuous network of endoplasmic reticulum in cerebellar Purkinje neurons. Proc Natl Acad Sci USA 91:7510–7514.

Thibault O, Landfield PW (1996) Increase in single L-type calcium channels in hippocampal neurons during aging. Science 272:1017–1020.

Varlinskaya EI, Spear LP (2008) Social interactions in adolescent and adult Sprague-Dawley rats: impact of social deprivation and test context familiarity. Behav Brain Res 188:398–405.

Verkhratsky A (2005) Physiology and Pathophysiology of the Calcium Store in the Endoplasmic Reticulum of Neurons. Physiological Reviews 85:201–279.

Wang Y, Deng X, Mancarella S, Hendron E, Eguchi S, Soboloff J, Tang XD, Gill DL (2010) The calcium store sensor, STIM1, reciprocally controls Orai and CaV1.2 channels. Science 330:105–109.

Wang Z, Xu N-L, Wu C-P, Duan S, Poo M-M (2003) Bidirectional changes in spatial dendritic integration accompanying long-term synaptic modifications. Neuron 37:463–472.

Weber JT (2012) Altered calcium signaling following traumatic brain injury. Front Pharmacol 3:60.

Xu C (2005) Endoplasmic reticulum stress: cell life and death decisions. Journal of Clinical Investigation 115:2656–2664.

Zhang W, Linden DJ (2003) The other side of the engram: experience-driven changes in neuronal intrinsic excitability. Nat Rev Neurosci 4:885–900.